

Evaluation of Reentry Effects of Delta II Second Stage Propellant Tanks

March 21, 2018

Gary L. Steckel¹ and Paul M. Adams²

¹Metals/Ceramics, Materials Science Department

²Material Physics and NDE, Materials Processing Department

Prepared for:

Space and Missile Systems Center
Air Force Space Command
483 N. Aviation Blvd.
El Segundo, CA 90245-2808

Contract No. FA8802-14-C-0001

Authorized by: Space Systems Group

Distribution Statement A: Approved for public release; distribution unlimited.



Abstract

Reentry effects were determined for two Delta II Stage 2 propellant tanks that reentered Earth's atmosphere. One of the tanks reentered on February 19, 2010 and landed near Buren, Mongolia. The tank was retrieved from Mongolia by AFSMC and provided to The Aerospace Corporation for a thorough metallurgical evaluation. Reentry effects were determined by visual observations, hardness measurements, and microstructural evaluations of mounted and polished cross-sections, including scanning electron microscopy with energy-dispersive x-ray spectroscopy for chemical analyses. Peak reentry surface temperatures were estimated at various locations on the cylindrical tank with domed ends. The other tank reentered and landed near Durbanville, South Africa on April 27, 2000. Although this tank was not retrieved by the USAF for evaluation, it was moved to and is on display at the South African Astronomical Observatory (SAAO) in Cape Town. Dr. Peter Martinez of the University of Cape Town generously provided photographs of the entire exterior surface of the South Africa tank to Aerospace for assessing its reentry condition. Reentry effects on the two tanks were compared to those documented by Aerospace in 2003 on a Delta II Stage 2 propellant tank that reentered over the United States on January 22, 1997 and landed in Texas. Common observations for the Texas, South Africa, and Mongolia debris included complete removal of an epoxy primer coating from the exterior surface, molten metal splatters at numerous locations on the tank surfaces, and localized melting along portions of the forward and aft ends of the cylindrical section due to enhanced aerodynamic heating at the exposed edges. A large hole through the forward dome wall was created by melting of the 410 stainless steel tank skin on the Texas and Mongolia tanks, but not on the South Africa tank. It was concluded that molten aluminum that splattered onto the propellant tanks from attachment hardware ignited and burned in the atmosphere. Burning aluminum added to frictional reentry heating caused localized melting of the stainless steel tanks. Peak reentry temperatures over most of the tank surface for the Mongolia tank were estimated at 1165° to 1215°C. Similar peak temperatures were previously reported for the Texas tank.

Contents

| | | |
|-------|--|----|
| 1. | Introduction..... | 1 |
| 2. | Background..... | 2 |
| 3. | Experimental Procedures..... | 4 |
| 4. | Results and Discussion..... | 5 |
| 4.1 | Review of C. C. Wan's Evaluation of the Propellant Tank Reentry in Texas..... | 5 |
| 4.2 | Physical Observations for the Propellant Tank Reentry in South Africa..... | 6 |
| 4.3 | Metallurgical Evaluation of the Propellant Tank Reentry in Mongolia..... | 7 |
| 4.3.1 | Physical Observations..... | 7 |
| 4.3.2 | Microstructural Evaluation and Hardness of 410 Stainless Steel at Various Locations on the Tank..... | 11 |
| 4.3.3 | SEM/EDS Analyses of 410 Stainless Steel Tank Locations with Reentry Melting..... | 13 |
| 4.3.4 | SEM/EDS Analyses for Determination of Peak Reentry Temperatures..... | 17 |
| 4.3.5 | Additional SEM/EDS Observations..... | 23 |
| 5. | Summary and Conclusions..... | 28 |

Figures

| | | |
|------------|--|----|
| Figure 1. | Photograph of Delta II 2nd stage vehicle. | 2 |
| Figure 2. | A sketch showing the construction of the Delta II Stage 2 propellant tank. | 3 |
| Figure 3. | Photograph of Delta II 2nd Stage propellant tank that reentered in 1997 and landed in Texas. | 5 |
| Figure 4. | Photographs of Delta II 2nd Stage propellant tank that reentered in 2009 and landed in Mongolia. | 8 |
| Figure 5. | Photographs of Mongolia propellant tank with concave side facing downward. | 8 |
| Figure 6. | Melting along ends of cylindrical section on concave side of Mongolia tank. | 9 |
| Figure 7. | Residual aluminum attached to forward end of cylindrical section and under rivets for Mongolia tank. | 9 |
| Figure 8. | Optical micrographs showing martensitic microstructures at various locations on the Mongolia tank. | 12 |
| Figure 9. | SEM/LABE image of an area on outer surface of tank cross-section at perimeter of melt-through hole. | 13 |
| Figure 10. | SEM/LABE image of an area on inner surface of tank cross-section at perimeter of melt-through hole. | 15 |
| Figure 11. | SEM/LABE image and quantitative EDS data for an area on outside surface of tank cross-section at forward edge of cylindrical section. | 17 |
| Figure 12. | Photograph of Sample B before cutting from region with resolidified metal splatters. | 18 |
| Figure 13. | Optical micrograph of cross-section of Sample B showing possible alloying between Al splatters and tank wall. | 19 |
| Figure 14. | Electron image and elemental maps of area in Figure 13. | 19 |
| Figure 15. | SEM/LABE image of polished cross-section showing region with alloying between Al splatters and tank wall. | 20 |
| Figure 16. | Iron–aluminum phase diagram. | 21 |
| Figure 17. | Magnified view of iron–aluminum phase diagram between 50 and 80 at. % Al. | 21 |
| Figure 18. | SEM/EDS elemental line across region with alloying between stainless steel tank and aluminum splatters. | 22 |
| Figure 19. | Photograph of Sample A1 secured to aft dome by binder clips after removal from Mongolia tank. | 24 |
| Figure 20. | Photographs of outside and inside surfaces of Sample A1. | 25 |
| Figure 21. | X-ray diffraction spectrum obtained from reddish oxide on Sample A1. | 25 |
| Figure 22. | X-ray diffraction spectrum obtained from gray oxide on Sample A1. | 26 |
| Figure 23. | LABE image of Cu-rich particles on top of aluminum splatters on Sample A3. | 27 |

Tables

| | | |
|----------|--|----|
| Table 1. | Extent of Melting or Erosion Around Forward and Aft Edges of Cylindrical Section of Propellant Tanks. | 10 |
| Table 2. | Samples for Laboratory Analyses. | 10 |
| Table 3. | Rockwell C Hardness at Five Locations on Mongolia Tank. | 11 |
| Table 4. | SEM/EDS Chemical Analysis on Outer Surface of Tank Wall at Perimeter of Melt-Through Hole. | 14 |
| Table 5. | SEM/EDS Chemical Analysis on Inner Surface of Tank Wall at Perimeter of Melt-Through Hole. | 16 |
| Table 6. | Summary of Peak Reentry Temperature Analyses at Several Locations on Mongolia Propellant Tank. | 23 |

1. Introduction

On February 24, 2010, The Aerospace Corporation's Center for Orbital and Reentry Debris Studies (CORDS) received an email from Nandin Baldorj, chief editor of Mongol News Media Group, reporting that space debris impacted a sparsely populated area in Mongolia on February 19, 2010. The email included 11 photographs of the debris, some of which showed close-up views of hardware serial numbers. From the serial numbers, the debris was determined to be from the second stage of a Delta II launch vehicle that was launched on September 25, 2009 from Cape Canaveral Air Force Station Launch Complex 17. The payload consisted of two demonstration satellites for the Space Tracking and Surveillance System (STSS). The satellites were placed in a circular, low-Earth orbit at an altitude of 1350 km [1].

Initially, two objects were found in a field approximately 30 km from Buren, located in central Mongolia, approximately 200 km southwest of Ulaanbaatar, the capital city of Mongolia. They landed in a dry, high desert region with sandy soil, small rocks, and no vegetation [2]. These objects have been identified to be the stainless steel cylindrical propellant tank (1.8-m diameter by 2.8-m long) and a titanium alloy spherical pressure vessel (43-cm diameter). A second, larger (61-cm diameter) titanium alloy pressure vessel was later found on the same trajectory approximately 100 km away. The pressure vessels were used for storage of nitrogen or helium gases.

A few days after the debris reentered Earth's atmosphere, Mongolian government personnel transported the three pieces of debris by truck to a military base in Ulaanbaatar. They were stored there until they were transferred to the U.S. Embassy 13 months later, on April 14, 2011 [2]. The large propellant tank was stored in an open or semi-open garage on the military base, while the Ti pressure vessels were stored indoors. All three debris pieces were stored in a semi-open area at the embassy [2]. The debris was retrieved by USAF personnel and delivered to Aerospace on August 30, 2011.

The stainless steel propellant tank is the second Delta II Stage 2 propellant tank to be retrieved by USAF and provided to Aerospace for evaluation. The first tank reentered over the U.S. and landed in Texas on January 22, 1997. It was delivered to Aerospace for evaluation in mid-April, 1998. The final report was published in 2003 [3].

Another Delta II Stage 2 propellant tank reentered and landed near Durbanville, South Africa on April 27, 2000 [4]. Although this tank was not retrieved by the USAF for evaluation, it was moved to and is on display at the South African Astronomical Observatory (SAAO) in Cape Town. Dr. Peter Martinez of the University of Cape Town generously provided photographs of the entire exterior surface of the South African tank to Aerospace for comparing its reentry condition with the Texas and Mongolia tanks.

At least one titanium alloy pressure vessel was retrieved for each of the three reentry events. None of the pressure vessels showed any evidence of significant reentry damage. As a result, no detailed evaluations were performed on any of the pressure vessels.

The objectives of this investigation were to document visible reentry damage to the propellant tanks that landed in South Africa and Mongolia, and to perform laboratory analyses on the Mongolia tank to characterize reentry damage and determine peak reentry temperatures. The final objective was to compare reentry damage between the propellant tanks that landed in Texas, South Africa, and Mongolia. Successfully completing these objectives will provide additional reentry effects data for analysts to employ in ongoing efforts to validate, refine, and calibrate reentry models for risk assessments.

2. Background

Figure 1 shows a photograph of a typical Delta II 2nd stage vehicle, also called the Delta-K stage. The large, pale green propellant tank is the primary structural element of the vehicle with the guidance system and miniskirt mounted of the forward end, and the Aerojet AJ10-118K engine mounted on the aft end. The helium and nitrogen pressure vessels are also mounted on the aft end.

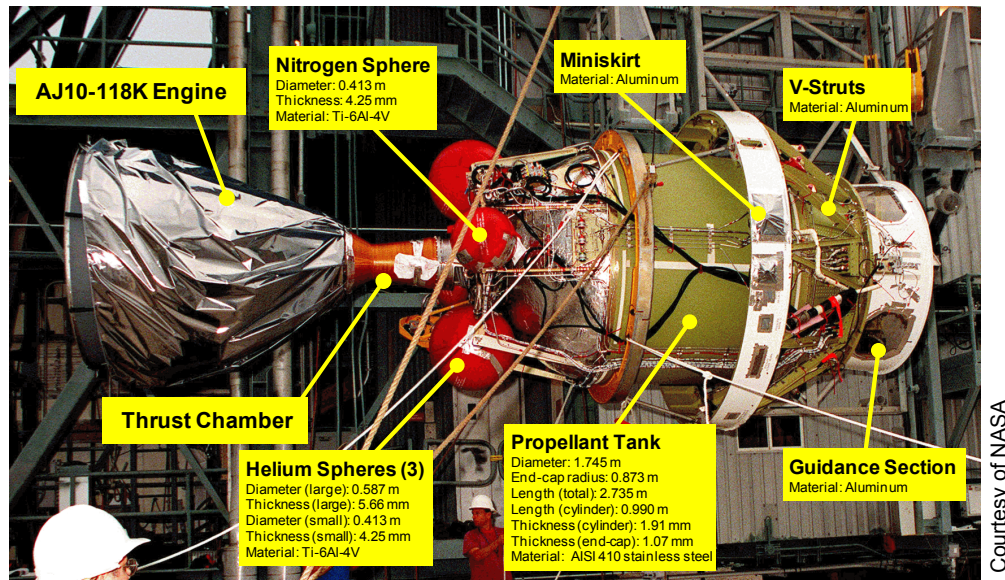


Figure 1. Photograph of Delta II 2nd stage vehicle.

Figure 2 shows a sketch of the propellant tank, previously shown in the final report for the Texas reentry [3]. The tank is a welded assembly consisting of forward and aft domes and a cylindrical midsection. It is divided into two chambers by an interior bulkhead, with Aerozine 50 fuel stored in the forward chamber and nitrogen tetroxide oxidizer in the aft chamber. The entire assembly is fabricated with 410 stainless steel. The domes are approximately 1.2-mm thick, and the cylindrical section is approximately 1.8-mm thick.

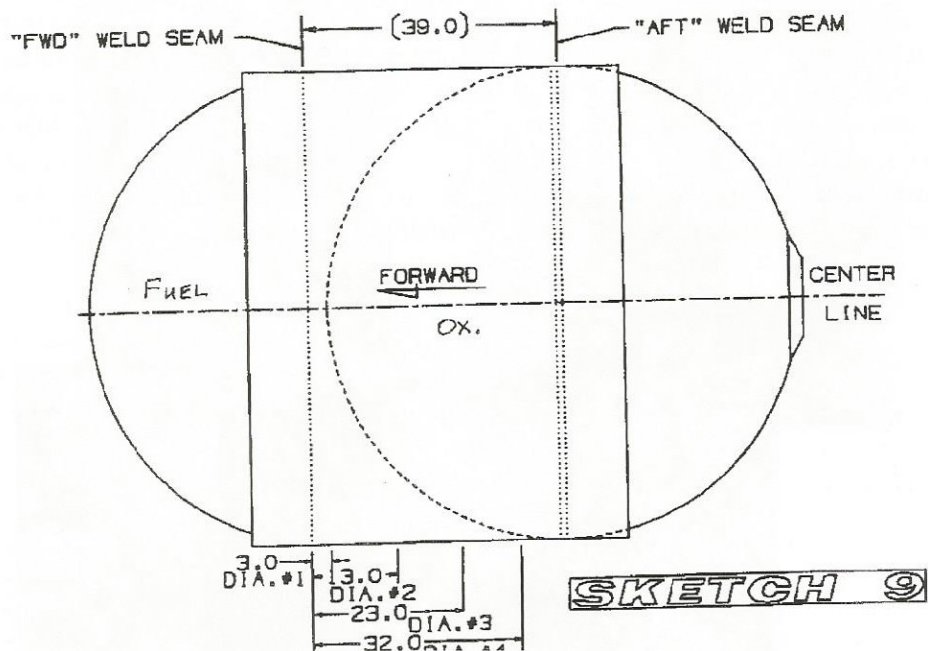


Figure 2. A sketch showing the construction of the Delta II Stage 2 propellant tank.

3. Experimental Procedures

The first step in the evaluation process for the Mongolia propellant tank was to document the physical condition of the tank via photographs and written notes. Photographs were taken using a high-resolution (2048 x 1536 pixel) digital camera with a zoom lens. The photographs were taken outdoors with natural lighting to best capture color variations.

Several areas on the tank were identified for detailed metallurgical analyses. Samples were removed from the stainless steel tank using an angle grinder equipped with 102-mm dia. by 1.14-mm thick abrasive cutting discs. The samples were carefully removed to avoid excessive heating—away from the immediate area of the cuts and to preserve the metallurgical condition of the areas for evaluation. Following extraction from the motor case, additional cross-sectioning of samples was performed using a slow-speed diamond wafer saw to eliminate the potential for heating or deformation damage. The saw was equipped with a 0.30-mm thick by 102-mm dia. blade. Cross-sections were mounted and polished, following standard metallographic procedures.

Surface topography and chemical composition of melted areas or areas with molten metal splatters were determined by scanning electron microscopy (SEM). A JEOL Model No. JSM-7600F SEM equipped with an energy dispersive x-ray spectrometer (EDS) was used for the analyses.

X-ray diffraction (XRD) analyses were performed using copper radiation with a PANalytical X'Pert Pro diffractometer equipped with an X'Celerator strip detector.

Microstructural analyses were performed on samples from several locations on the tank including the perimeter of a large melt-through hole, areas with a heavy build-up of resolidified molten metal splatters on the surface, and areas with little to no molten metal splatter. These analyses were performed to compare the microstructures of the base stainless steel at the different locations, and to determine the extent of alloying between the molten metal splatters and the stainless steel. SEM/EDS analyses of the areas with alloying were used to estimate peak reentry temperatures at various locations on the tank.

Optical microscopy was performed using a Nikon, Inc. EPIPHOT inverted metallurgical microscope. The microscope was equipped with a digital camera eyepiece and software for capturing digital images with a maximum resolution of 1280 x 1024 pixels. Mounted and polished 410 stainless steel samples were etched for microstructural analyses using Vilella's reagent (5 ml HCl, 1 g picric acid, and 100 ml 95% ethanol) [5]. Samples were typically etched by immersion in the reagent for 30 to 45 sec.

Hardness measurements were made on many of the samples that were cut from the motor cases for microstructural analyses. Rockwell Superficial 30N scale hardness measurements were made on the inside and outside surfaces of the tank samples prior to cross-sectioning. Surface corrosion was lightly sanded away prior to the measurements, using 240-grit abrasive paper.

4. Results and Discussion

4.1 Review of C. C. Wan's Evaluation of the Propellant Tank Reentry in Texas

Following analysis, the propellant tank from the Texas reentry was maintained at Aerospace and is on display at the corporate headquarters in El Segundo, CA. Figure 3 shows a photographic view from the aft end of the propellant tank mounted on the display base. As discussed in Reference [3], one side of the tank (bottom side in Figure 3) was flattened, presumably due to Earth impact. The force of the impact on the hot, softened tank skin also caused partial flattening of the top side. A long circumferential crack around the rear side of the aft dome was also attributed to Earth impact. Only the upper end of this crack is visible in Figure 3. None of hardware attached to the tank, as shown in Figure 1, remained after reentry, although portions of welded hardware brackets were still present.

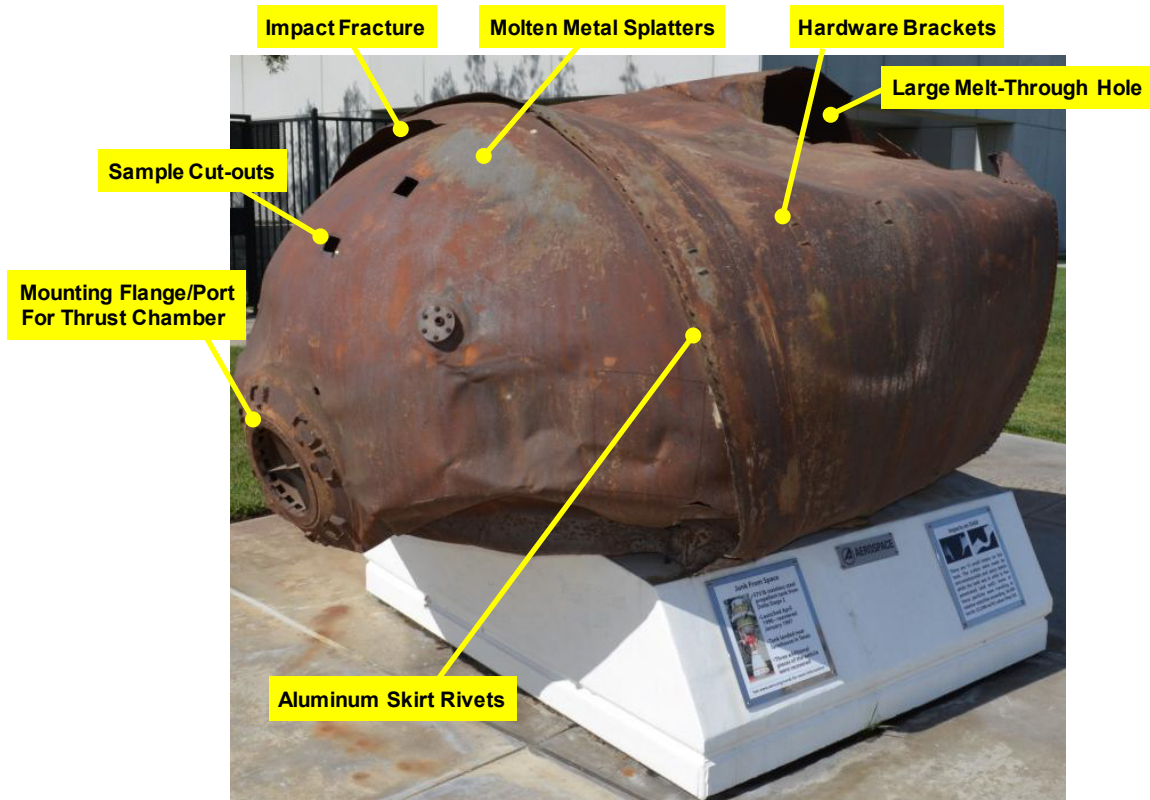


Figure 3. Photograph of Delta II 2nd Stage propellant tank that reentered in 1997 and landed in Texas.

A large hole with an area around 0.5 m^2 was present on the upper side of the forward dome. It was concluded from the presence of resolidified metal around the perimeter of the hole that the stainless steel skin had melted at this localized area during reentry. However, such gross melting of the stainless steel skin, which occurs at approximately 1500°C , was not observed at any other location on the tank. There were, however, splatters of various sizes of resolidified molten metal at several locations on the tank surface. It was determined from SEM/EDS analyses that these splatters were primarily aluminum. It was concluded that aluminum hardware attached to the Stage II tank had melted during reentry and landed on the tank surface. Since aluminum alloys melt at approximately 660°C , it was concluded from these observations that the peak reentry temperature of the tank was at least 660°C , but less than 1500°C .

As shown in Figure 1, the Delta II Stage II propellant tank is launched with a pale green epoxy primer on the external surface. There was no visible trace of this coating on the tank after reentry. It was concluded that the epoxy primer either spalled off from thermal stresses or burned off during reentry.

Many small, circular holes ranging from 2 to 3 mm dia. were observed on the tank skin. A total of 17 holes were found, 15 on the aft dome and 2 on the cylindrical section. Four of the 17 holes penetrated through the tank skin, while most of the holes were crater-like depressions. It was concluded that the small holes were the result of impacts by micrometeoroids or tiny space debris while the tank was in orbit.

Other observations included erosion or partial melting of stainless steel rivets, where aluminum alloy hardware was attached around the forward and aft ends of the cylindrical section and brackets at various locations around the cylindrical section. The melting or erosion was attributed to extreme aerodynamic heating at these irregularities on the tank surface.

Cross-sections of the stainless steel tank skin in locations with resolidified molten aluminum splatters on the surface revealed alloying between the Fe-rich stainless steel and the molten Al. SEM/EDS analyses were used to identify Al-Fe intermetallic phases formed. The microstructures of these phases indicated that some of them were molten during reentry, while others remained solid. From the Al-Fe phase diagram, the peak reentry temperature was estimated from the relative compositions of phases with and without reentry melting. Analyses of samples from the aft and forward domes indicated similar temperatures of 1200–1280°C when the tank landed. This same approach was used to estimate peak reentry temperatures at multiple locations on the tank that reentered in Mongolia and will be discussed in detail in section 4.3.4.

Given a peak reentry temperature of 1280°C on the forward dome a short distance from the large melt-through hole, additional analyses were needed to explain the localized melting of the stainless steel skin. SEM/EDS analyses of the resolidified metal around the perimeter of the hole indicated highly oxidized Fe and Cr—the primary constituents of 410 stainless steel—at the interior surface, but highly oxidized Al with very little Fe and Cr at the exterior surface. Furthermore, the external surface had a burned, black appearance. From these observations, it was theorized that, during reentry, molten aluminum from melting hardware spread over the forward dome and subsequently caught on fire. Heat generated by the burning aluminum increased the local temperature above the melting point of the stainless steel tank skin. Evidence of this mechanism has also been observed at melt-through holes on titanium alloy motor cases for five Delta II Upper Stage reentry events [6]–[8].

4.2 Physical Observations for the Propellant Tank Reentry in South Africa

Unfortunately, we were unable to contact Dr. Martinez to obtain permission to include the University of Cape Town photographs in this report. Consequently, observations for the South African propellant tank are presented without the benefit of supporting photographs. The photographs show that one side of the tank was flattened by Earth impact, while the cylindrical section on the opposite side and spherical domes were relatively undeformed. The general post-reentry shapes of the South Africa and Texas tanks, flat on one side and relatively undeformed around the remainder of the circumference, were similar. However, whereas a long crack—nearly 180° around the aft dome—was present on the Texas tank, no long cracks were observed on the South Africa tank. Wan suggested that the lack of significant deformation around the tank was evidence that the tank did not bounce or roll along the ground after the initial impact [3]. However, inspection of the area around the final resting location of the South Africa tank revealed heat damage to sparse grass for a considerable distance, along a path consistent with the direction of the reentry trajectory [4]. Thus, it was concluded that the stainless steel tank probably bounced, rolled, and tumbled for a considerable distance after impact.

Other similarities between the Texas and South Africa tanks included complete removal of the pale green epoxy primer, molten metal splatters at numerous locations, and melting or erosion of some of the stainless steel rivets at the ends of the cylindrical section. Both tanks had a clean separation from the thrust chamber and AJ10-118K engine at the aft flange. It is assumed that this separation occurred during structural breakup of the vehicle early in reentry.

Several small impact craters from orbital space debris or micrometeorite impacts were reported on the external surface of the South Africa tank [4]. Unfortunately, the exact number and specific locations of the impact craters were not reported to allow comparison with the craters on the Texas tank.

It is apparent from Figure 3 that the Texas tank has a dark rusty appearance, and it will be shown in section 4.3.1 that the Mongolia tank has a similar appearance. The photographs of the South Africa tank revealed that it has a lighter brown color. The 410 stainless steel alloy has a martensitic structure that is susceptible to atmospheric corrosion. The Texas and Mongolia tanks have been stored outdoors for many years, while the South Africa tank was relocated indoors at SAAO shortly after recovery. Thus, the rusty appearance of the Texas and Mongolia tanks are indicative of their post-reentry storage history.

It was determined from the photographs that the South Africa tank survived reentry without incurring any large melt-through holes. It is the only tank out of three recovered Delta II Stage 2 stainless steel propellant tanks and five recovered Delta II Upper Stage titanium motor cases with no large melt-through holes.

4.3 Metallurgical Evaluation of the Propellant Tank Reentry in Mongolia

4.3.1 Physical Observations

A set of four photographs in Figure 4 show the forward and aft ends and opposing side views of the Mongolia propellant tank. The tank was more grossly deformed than the Texas and South Africa tanks. One side totally collapsed into a concave bowl shape; it is assumed that initial Earth impact was on this side. An arbitrary coordinate system, as shown on the forward end photo, was used to define relative angular positions around the cylindrical tank. The center of the concave side was defined as 0°. Figure 5 shows a second set of four photographs taken with the concave side facing downward. These photos show very little deformation on the upper side of the tank at the forward end, but at the aft end they show flattening into an oval shape. The aft end photos in Figures 4 and 5 show that the aft dome was almost completely missing and the bulkhead that separated the fuel and oxidizer chambers was pushed outward through the remnants of the aft dome. The jagged edge of the dome remnants suggest that the dome fractured circumferentially a short distance behind the welded interface to the cylindrical section. Heating damage was observed around much of the fracture surface, suggesting that the dome probably fractured during breakup of the Stage 2 vehicle in the early stage of reentry. This likely occurred when the thrust chamber and engine were ripped away from the tank. Whereas clean separation between the tank and thrust chamber occurred at the mounting flange for the Texas and South Africa tanks, separation for the Mongolia tank occurred by failure of the stainless steel dome skin. The structural integrity of the tank was greatly diminished by removal of the aft dome. This probably allowed the tank to collapse into a concave shape upon Earth impact.

The deformed tank was approximately 2 m long by 2 m wide, with a height of 0.8 m at the aft end and 1.3 m at the forward end. The mass of the recovered tank was 205 kg.

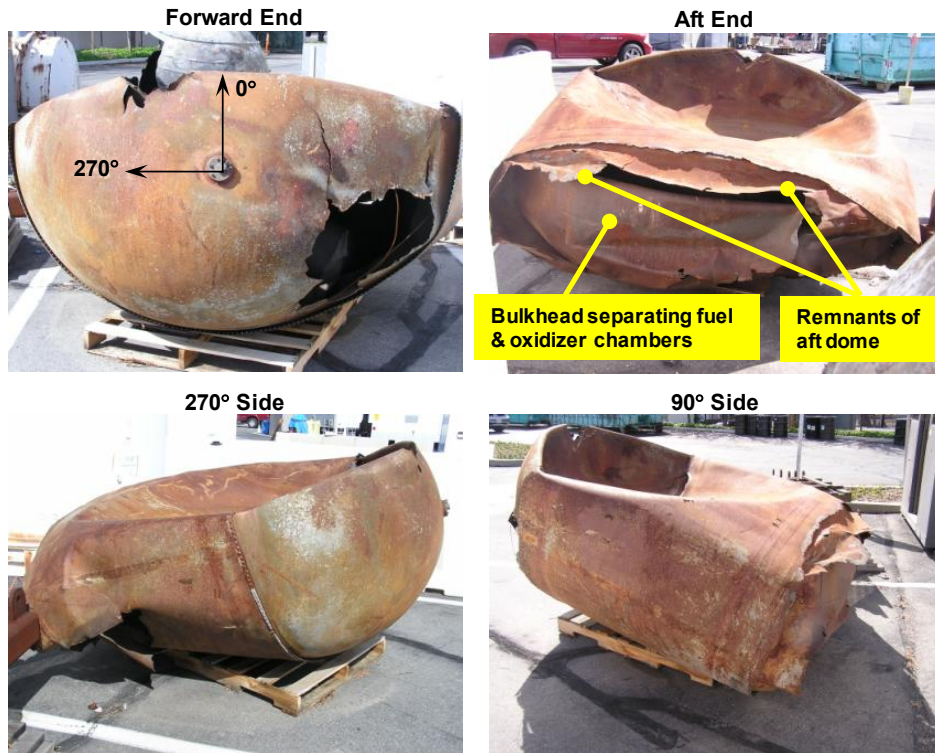


Figure 4. Photographs of Delta II 2nd Stage propellant tank that reentered in 2009 and landed in Mongolia.



Figure 5. Photographs of Mongolia propellant tank with concave side facing downward.

A large melt-through hole was observed on the forward dome, as shown in the forward end photo in Figure 4. The hole was similar in size ($\cong 0.5 \text{ m}^2$) and location to the melt-through hole on the Texas tank. Furthermore, the perimeter of the melt-through hole consisted of resolidified metal, appeared to have aluminum splatters on the external surface, and was curled outward. All observations were consistent with the hole on the Texas tank. A second, smaller melt-through hole is visible in Figure 4, near the center of the forward dome at the rim of the concave deformation. It is not surprising that the melt-through holes for both tanks were on the forward dome. As shown in Figure 1, a large aluminum housing joining the propellant tank to the guidance section is riveted to the forward end of the cylindrical section, while only a short aluminum skirt is riveted to the aft end. Thus, the potential for heavy molten aluminum splatters and aluminum burning is much higher for the forward dome.

Widespread melting or erosion of the forward and aft ends of the cylindrical section back through the stainless steel rivets occurred on the concave side of the tank (Figure 6). On the other hand, very little melting or erosion of cylinder ends occurred around the opposite side ($\cong 70^\circ\text{--}290^\circ$). Furthermore, as shown in Figure 7, residual aluminum remained under the rivets, along a portion of the forward end of the cylindrical section.

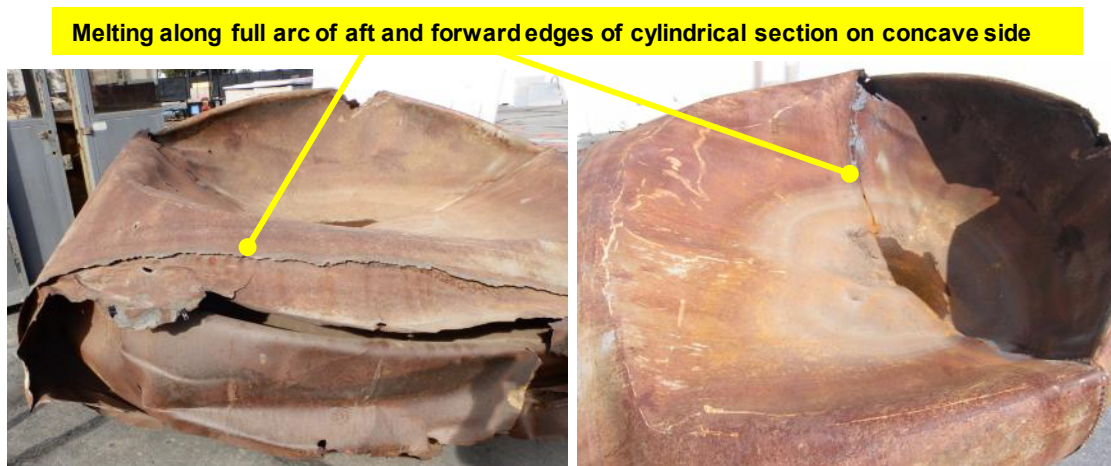


Figure 6. Melting along ends of cylindrical section on concave side of Mongolia tank.

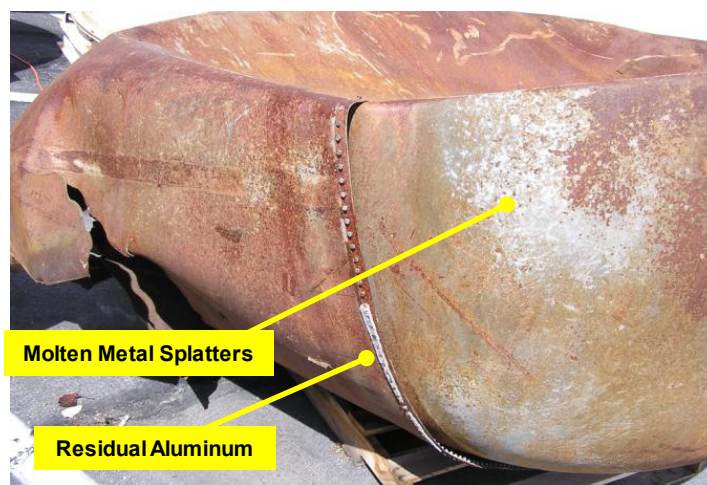


Figure 7. Residual aluminum attached to forward end of cylindrical section and under rivets for Mongolia tank.

A close inspection of the photographs of the South Africa tank revealed that it also had preferential melting or erosion of the forward and aft ends of the cylindrical section on the flattened, impact side relative to the undeformed side. The extent of melting along the cylindrical section edges on the flat/concave side versus the relatively undeformed round side is quantified in Table 1 for all three propellant tanks. The Mongolia and South Africa tanks clearly had more edge melting on the flat or concave side. The Texas tank showed no preference for cylinder edge melting on the flat side, but had a strong preference for melting along the aft cylinder end rather than the forward end. These observations may be an indication that each of the three tanks had a preferential leading side during reentry. On the other hand, it could be due to unquantifiable differences in the factors affecting the complex aerodynamic air flow around the cylinder edges. Presently, no definitive conclusions can be reached from these observations.

Table 1. Extent of Melting or Erosion Around Forward and Aft Edges of Cylindrical Section of Propellant Tanks

| Circumferential Location | End of Cylindrical Section | Percentage of Cylinder Circumference with Edge Melting | | |
|--------------------------|----------------------------|--|-------------------|---------------|
| | | Texas Tank | South Africa Tank | Mongolia Tank |
| Flat or Concave Side | Forward | 0 | 60 | 100 |
| | Aft | 100 | 100 | 100 |
| Round Side | Forward | 10 | 0 | 0 |
| | Aft | 85 | 15 | 0 |

Based on the physical observations, several locations on the tank were selected for the extraction of samples for laboratory analyses. The samples are listed in Table 2, along with their locations on the tank and accompanying analyses performed. Sections 4.3.2 through 4.3.4 discuss the results.

Table 2. Samples for Laboratory Analyses

| Sample No. | Sample Description | Location on Propellant Tank | | Analyses |
|------------|----------------------------------|---|-----------------|--|
| | | Axial | Circumferential | |
| A1 | Aft Dome Remnant with Gray Color | Fracture Surface of Aft Dome | 45° | X-ray Diffraction, Microstructure, SEM/EDS |
| A2 | Edge Melting | Forward Cylinder Edge | 45° | Hardness, Microstructure, SEM/EDS |
| A3 | Resolidified Metal Splatters | Forward Dome, 24 cm from Cylinder Edge | 270° | Hardness, Microstructure, SEM/EDS |
| B | Resolidified Metal Splatters | Cylinder Wall, 20 cm Aft of Forward Edge | 90° | Hardness, Microstructure, SEM/EDS |
| C | Resolidified Metal Splatters | Cylinder Wall, 25 cm Forward of Aft Edge | 75° | Hardness, Microstructure, SEM/EDS |
| D | Resolidified Metal Splatters | Forward Dome, 5 cm from Cylinder Edge, 10 cm from Melt-Through Hole | 90° | Hardness, Microstructure, SEM/EDS |

| Sample No. | Sample Description | Location on Propellant Tank | | Analyses |
|------------|-----------------------------|---------------------------------------|-----------------|-----------------------------------|
| | | Axial | Circumferential | |
| H | Melt-Through Hole Perimeter | Forward Dome, 5 cm from Cylinder Edge | 100° | Hardness, Microstructure, SEM/EDS |
| J | Aft Dome Remnant | Fracture Surface of Aft Dome | 0° | Hardness |

4.3.2 Microstructural Evaluation and Hardness of 410 Stainless Steel at Various Locations on the Tank

Table 3 provides hardness data for Sample Nos. H, J, A3, A2, and C. Measurements were made at three points on the outside and inside surfaces for each sample. The average values and standard deviations for both surfaces are given in the table. Sample Nos. H and A3 were taken from the forward dome, with Sample H cut from the perimeter of the melt-through hole and Sample A3 cut from an area far away from the melt-through. Sample Nos. A2 and C were taken from the cylinder wall, with Sample A2 cut from the forward edge and Sample C from an area 25 cm forward of the aft edge. Sample J was from the aft dome. Although average hardness values varied significantly from around 44 to 55 HRC, all the values are quite high for 410 stainless steel. Tempered martensite for 410 stainless steel has typical hardness values between 43 HRC for low-tempering temperatures ($\cong 200^{\circ}\text{C}$) and 35 HRC for high-tempering temperatures (540°C) [9]. Thus, the hardness values in Table 3 are indicative of untempered martensite. It is highly unlikely that the tank was fabricated in this condition, due to the low ductility of untempered martensite. It is therefore concluded that reentry heating was sufficient to transform the microstructure from the initial tempered martensite to austenite. When the tank slowly cooled after landing, it transformed to untempered martensite. The standard heat treatment for austenitizing 410 stainless steel is 980°C for one hour [9]. Considering the short time for reentry heating, the peak reentry temperature had to be well over 1000°C to enable complete transformation to austenite. The analyses presented in section 4.3.4 will verify that reentry temperatures were sufficient to austenitize the stainless steel tank wall.

Table 3. Rockwell C Hardness at Five Locations on Mongolia Tank

| Location | Rockwell C Hardness | | | | | | | | | |
|----------|---------------------|------|----------|------|-----------|------|-----------|------|----------|------|
| | Sample H | | Sample J | | Sample A3 | | Sample A2 | | Sample C | |
| | ID | OD | ID | OD | ID | OD | ID | OD | ID | OD |
| Point 1 | 48.4 | 52.3 | 46.4 | 44.7 | 44.0 | 45.3 | 55.5 | 53.9 | 48.3 | 48.5 |
| Point 2 | 48.2 | 50.4 | 41.7 | 48.7 | 45.2 | 45.2 | 54.1 | 53.6 | 48.5 | 49.4 |
| Point 3 | 49.5 | 49.4 | 44.6 | 46.4 | 44.6 | 46.2 | 54.6 | 51.9 | 48.3 | 49.0 |
| Average | 48.7 | 50.7 | 44.2 | 46.6 | 44.6 | 45.6 | 54.7 | 53.1 | 48.4 | 49.0 |
| St. Dev. | 0.7 | 1.5 | 2.4 | 2.0 | 0.6 | 0.6 | 0.7 | 1.1 | 0.1 | 0.5 |

The highest hardness values were measured for Sample Nos. H and A2. These samples were cut from areas immediately adjacent to the melt-through hole and molten edge of the cylinder wall, respectively. These samples undoubtedly reached higher temperatures than the samples from the other locations on the tank. The higher austenitizing temperature probably led to higher hardness values.

Seven of the eight samples listed in Table 2, excluding Sample J, were cross-sectioned, mounted, polished, and etched for evaluation of post-reentry microstructures by optical microscopy. Figure 8 shows four micrographs that represent the microstructures observed for the samples from the seven different tank locations. The upper left micrograph in Figure 8 is representative of all the areas on the tank that had no melting of the stainless steel during reentry (Sample Nos. A1, A3, B, C, and D). This is the lath martensite structure typical of 410 stainless steel. The orientation of the lathes differs for individual prior austenite grains. It follows that the prior austenite grains had diameters in the range of 20 to 40 μm . The upper right and lower right micrographs show the same microstructure as the upper left, but with larger prior austenite grain sizes. The upper right micrograph is of an area near the cylinder wall edge that melted during reentry, but with no surface melting. The lower right micrograph represents areas with surface melting. Progressively higher peak temperatures at the locations of the upper left to upper right to lower right micrographs caused increasing amounts of austenite grain growth. Prior austenite grain diameters were around 30 to 50 μm for the upper right microstructure, and over 150 μm for the lower right micrograph.

The lower left micrograph shows a unique microstructure observed near the melt-through hole on Sample H. The dark areas are lath martensite, and the white areas are retained austenite at the prior austenite grain boundaries that did not transform during post-reentry cooling. This microstructure clearly shows the prior austenite grain size, similar to that in the upper right micrograph. The cause of the retained austenite was not pursued, but could be due to carbon or chromium depletion at the grain boundaries.

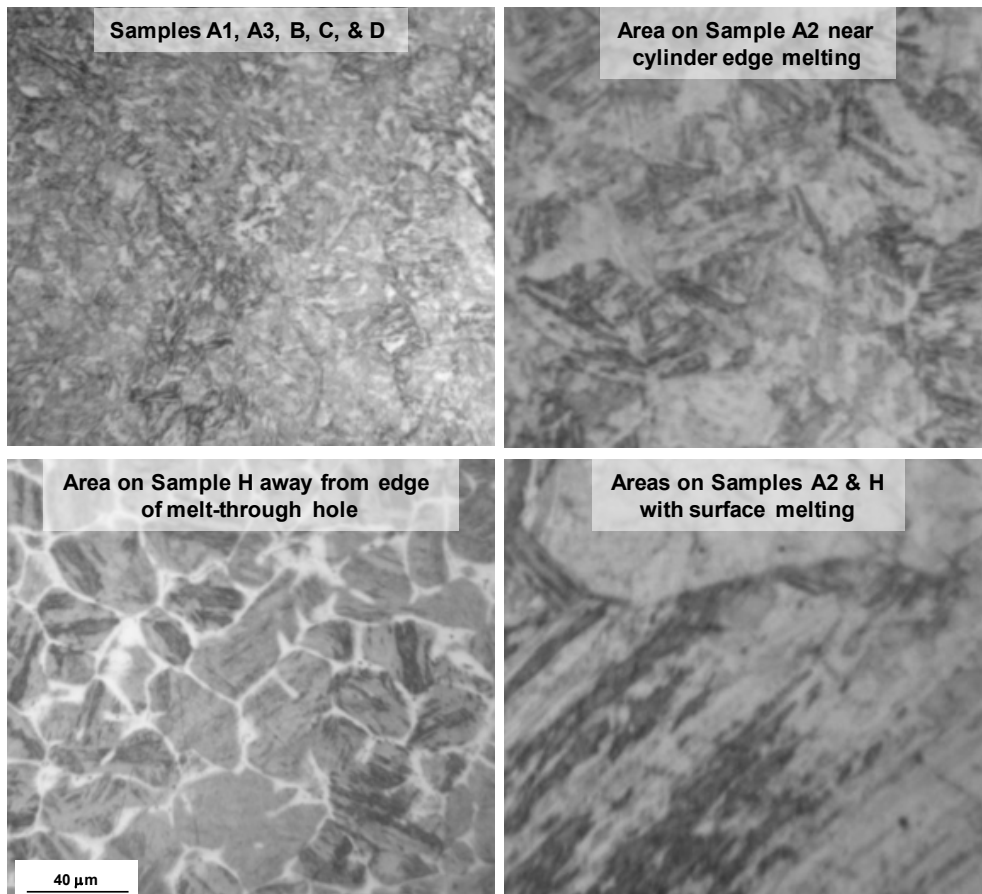


Figure 8. Optical micrographs showing martensitic microstructures at various locations on the Mongolia tank.

4.3.3 SEM/EDS Analyses of 410 Stainless Steel Tank Locations with Reentry Melting

Melting of the 410 stainless steel tank was observed at two general locations, a large melt-through hole on the forward dome and along the forward and aft edges of the cylindrical section. Based on previous results for the Texas tank [3], the Aerospace team believes two different mechanisms were responsible for the localized melting. The melt-through on the forward dome was likely caused by a layer of molten aluminum that splattered onto the tank from aluminum alloy hardware catching on fire in the oxidizing air stream, whereas melting along the ends of the cylindrical section was caused by enhanced frictional heating at the exposed metal edges. To validate these mechanisms, SEM/EDS analyses were performed on cross-sections of resolidified metal cross-sections from Sample A2 at the cylinder edge and Sample H at the perimeter of the melt-through hole.

The polished cross-section of Sample H was analyzed in the SEM using EDS to determine the chemical composition of the resolidified metal near the edge of the melt-through hole on the outside and inside surfaces of the tank wall. Figure 9 is a low-angle backscatter electron (LBE) image of an area on the outside surface. The image is centered 3 mm to the left of the edge of the hole.

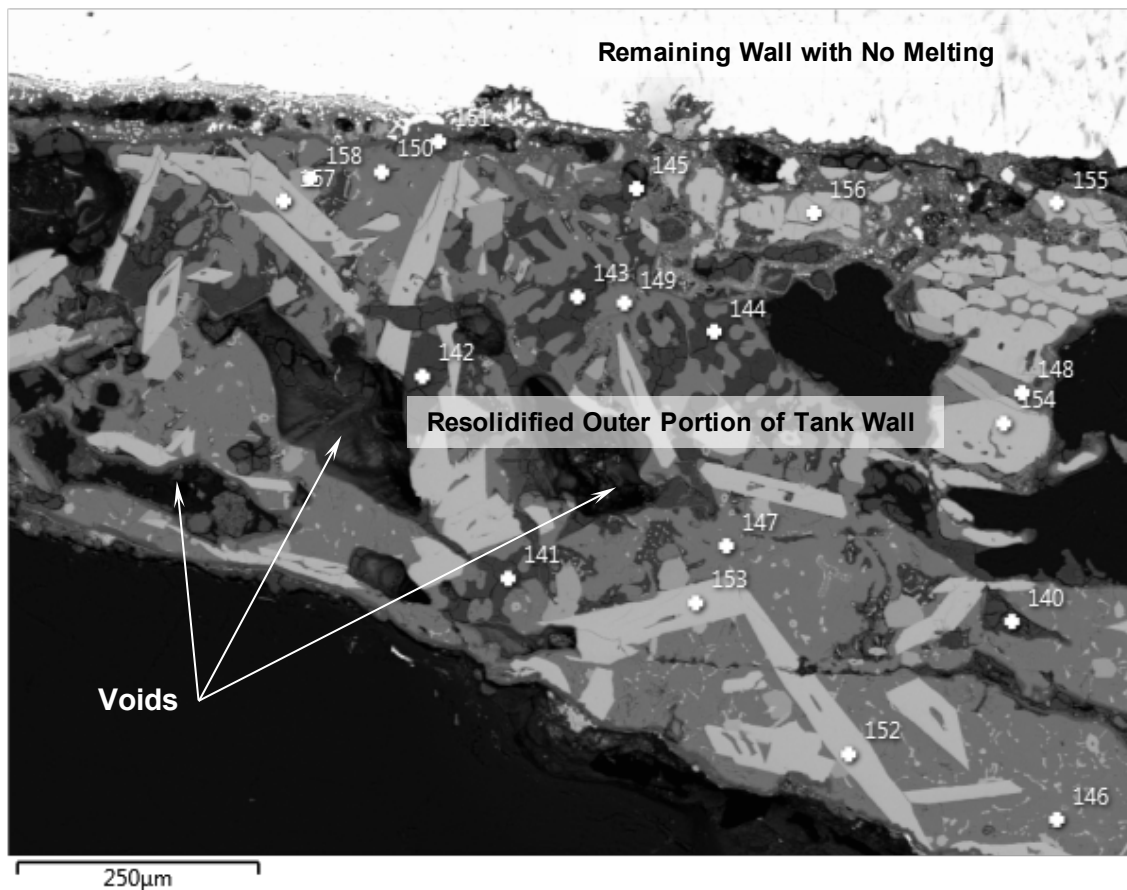


Figure 9. SEM/LBE image of an area on outer surface of tank cross-section at perimeter of melt-through hole.

In this backscatter electron image, high atomic number constituents appear brighter than lower atomic number constituents. The bright area at the top of the image is an interior region of the stainless steel tank wall that did not melt during reentry. The porous material below the remaining wall is a layer of resolidified metal on the outer surface of the tank wall. It is composed of three different phases, with differing atomic weights yielding three distinct shades of gray in the image. The primary phase is a

neutral gray tone with patches of a dark gray phase having a dendritic appearance and a light gray phase having mostly a platelet morphology. The black areas within the porous resolidified metal are voids. EDS spectra were taken at 19 points within the resolidified metal labeled points 140 – 158. Table 4 shows the tabulated results of the EDS analyses. The primary phase (neutral gray areas, Points 146–150) consisted of essentially elemental aluminum with small amounts of iron, chromium, and silicon from the stainless steel wall and around 3 at.% oxygen. The dark gray phase (Points 140–145 & 151) consisted of fully oxidized aluminum (\cong 37 at.% Al and 61 at.% O). The light gray platelet phase consisted of an alloyed mixture of aluminum and 410 stainless steel consisting of approximately 77 at.% Al, 20 at.% Fe, and small amounts of Cr and Si.

Table 4. SEM/EDS Chemical Analysis on Outer Surface of Tank Wall at Perimeter of Melt-Through Hole

| Element | Elemental Concentration, atomic % | | | | | | | | | |
|---------|-----------------------------------|------|------|------|------|------|------|------|---------|----------|
| | Dark Gray Areas | | | | | | | | Average | St. Dev. |
| | 140 | 141 | 142 | 143 | 144 | 145 | 151 | | | |
| Al | 31.6 | 33.5 | 27.2 | 40.4 | 35.5 | 29.1 | 57.6 | 36.4 | 10.3 | |
| Fe | 0.0 | 0.0 | 0.2 | 0.0 | 0.0 | 0.5 | 0.3 | 0.1 | 0.2 | |
| O | 65.7 | 64.8 | 69.4 | 57.3 | 62.5 | 66.2 | 40.0 | 60.8 | 9.9 | |
| Cr | 0.0 | 0.0 | 0.0 | 0.0 | 0.0 | 0.0 | 0.3 | 0.0 | 0.1 | |
| Si | 0.3 | 0.2 | 0.3 | 0.3 | 0.3 | 2.6 | 1.8 | 0.8 | 1.0 | |
| Mg | | | | 0.3 | | | | 0.3 | | |
| Cl | 0.8 | 1.1 | 0.8 | 0.9 | 1.4 | 1.0 | | 1.0 | 0.2 | |
| S | 1.6 | 0.4 | 2.1 | 0.8 | 0.3 | 0.6 | | 1.0 | 0.7 | |
| Element | Neutral Gray Areas | | | | | | | | Average | St. Dev. |
| | 146 | 147 | 148 | 149 | 150 | | | | | |
| Al | 96.3 | 95.5 | 95.2 | 95.5 | 96.0 | | | 95.7 | 0.4 | |
| Fe | | | | | 0.2 | | | 0.2 | | |
| O | 3.0 | 3.4 | 3.5 | 3.2 | 2.7 | | | 3.2 | 0.3 | |
| Cr | | | | | 0.1 | | | 0.1 | | |
| Si | 0.7 | 1.1 | 1.3 | 1.3 | 1.0 | | | 1.1 | 0.2 | |
| Element | Light Gray Areas | | | | | | | | Average | St. Dev. |
| | 152 | 153 | 154 | 155 | 156 | 157 | 158 | | | |
| Al | 75.7 | 76.2 | 75.8 | 75.5 | 75.0 | 76.3 | 86.1 | 77.2 | 3.9 | |
| Fe | 22.7 | 22.0 | 22.1 | 21.9 | 22.6 | 22.3 | 4.1 | 19.7 | 6.9 | |
| O | | | | | | | | | | |
| Cr | 0.9 | 1.1 | 1.3 | 1.7 | 1.3 | 0.9 | 9.1 | 2.3 | 3.0 | |
| Si | 0.7 | 0.7 | 0.8 | 0.9 | 1.1 | 0.5 | 0.7 | 0.8 | 0.2 | |

Figure 10 shows an SEM/LABE image of an area on the inside of the tank wall approximately 5 mm from the edge of the melt-through hole. Table 5 presents the results of EDS spectra at Points 1–5. The light gray area represented by Point 5 consists of remaining unmelted stainless steel wall. The gray inner layer of resolidified material (\cong 30–80 μ m thick, Pts. 3 & 4) was highly oxidized with equal amounts of iron and chromium. The darker gray outer layer (\cong 10–40 μ m thick, Pts. 1 & 2) was mostly iron oxide. The inner surface of the tank was not accessible to molten metal splatters, so very little aluminum was present. The

high concentration of Cr in the inner oxide layer can probably be attributed to the fact that Cr_2O_3 has a much lower free energy of formation at the melting temperature of 410 stainless steel than any of the potential iron oxides (FeO , Fe_2O_3 , or Fe_3O_4). Thus, an oxide layer rich in Cr formed first. Once the available Cr was all oxidized, free Fe atoms diffused through the inner oxide layer to react with oxygen to form the outer oxide layer.

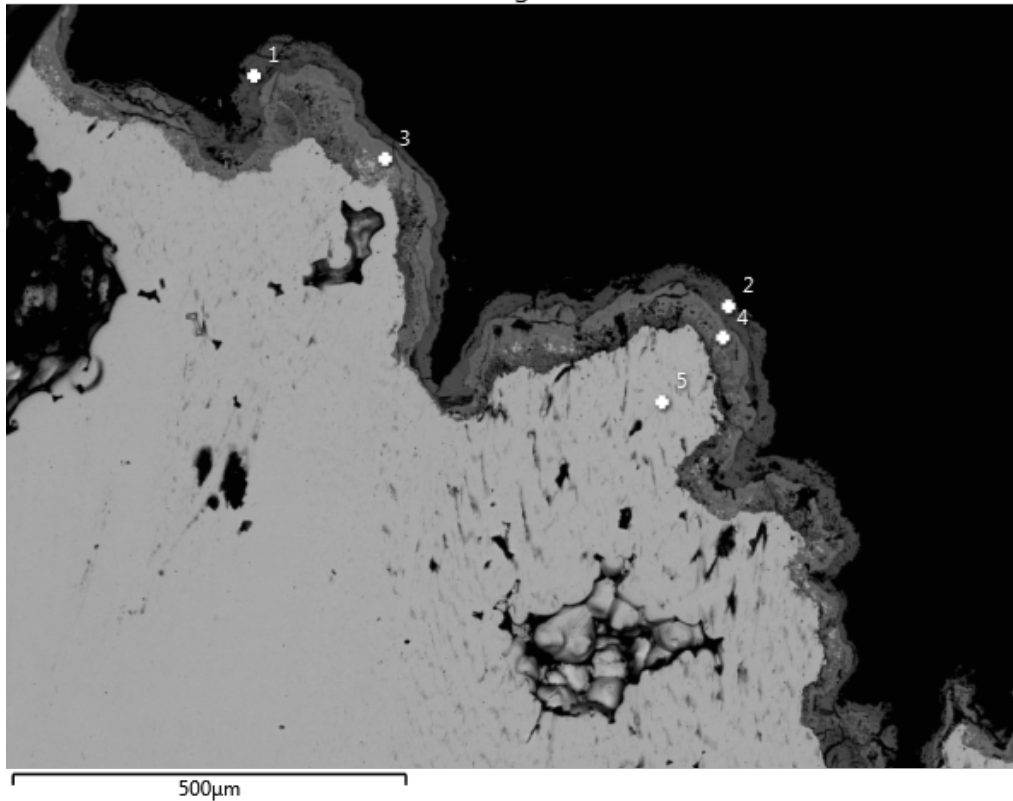


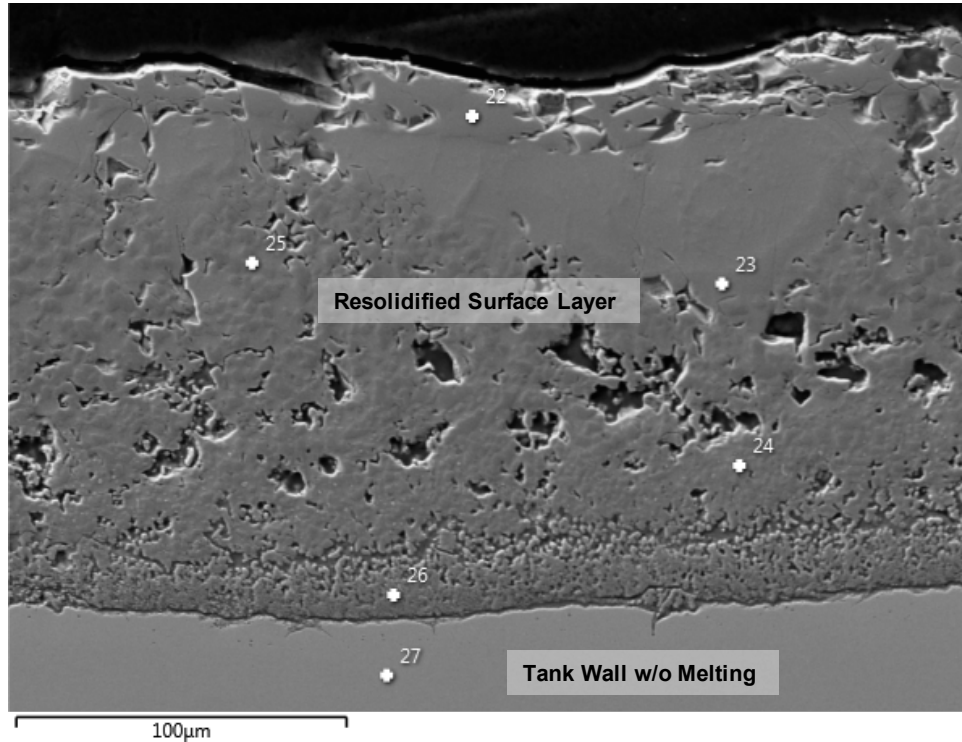
Figure 10. SEM/LABE image of an area on inner surface of tank cross-section at perimeter of melt-through hole.

Table 5. SEM/EDS Chemical Analysis on Inner Surface of Tank Wall at Perimeter of Melt-Through Hole

| Element | Elemental Concentration, atomic % | | | | |
|---------|-----------------------------------|------|------|------|------|
| | 1 | 2 | 3 | 4 | 5 |
| Al | | | 0.6 | 0.7 | |
| Fe | 32.5 | 32.0 | 19.7 | 17.3 | 88.1 |
| O | 66.3 | 67.1 | 57.1 | 58.2 | |
| Cr | 0.4 | 0.2 | 19.9 | 21.6 | 11.5 |
| Mn | | | 1.0 | 0.9 | |
| Si | | 0.2 | 1.7 | 1.3 | 0.4 |
| Cl | 0.6 | 0.5 | | | |
| S | 0.2 | | | | |

The SEM/EDS results for the resolidified metal on the outside and inside surfaces of the tank cross-section at the perimeter of the melt-through hole are consistent with those reported by Wan [3] for the Texas reentry. Thus, the current results support his hypothesis that aluminum hardware attached to the propellant tank melted and splattered onto the forward dome of the tank, subsequently caught on fire due to rapid oxidation by the air stream, and generated sufficient heat to cause localized melting through the tank dome.

Figure 11 shows an SEM/LABE image of a polished cross-section of Sample A2 from the forward edge of the cylindrical section. The lower area consists of remaining wall thickness that did not melt, and the porous upper area consists of resolidified metal on the outside surface. The results of EDS spectra taken at Points 22–27 are tabulated at the bottom of the figure. The resolidified metal was highly oxidized throughout the thickness, but was mostly iron oxide near the free surface (points 22, 23, & 25), with higher concentrations of chromium present near the remaining tank wall (Points 24 & 26). Although some aluminum was present, the concentrations were low, and there was no evidence of aluminum burning contributing to the tank melting. Similar results were obtained at five other areas on the cross-section. The results were consistent, with the assumption that melting was due to enhanced aerodynamic heating at the exposed cylinder edge.



| Element | Elemental Concentration, atomic % | | | | | |
|---------|-----------------------------------|------|------|------|------|------|
| | 22 | 23 | 24 | 25 | 26 | 27 |
| O | 55.7 | 53.1 | 53.8 | 55.0 | 58.3 | |
| Al | | | 0.9 | 1.6 | 0.8 | |
| Si | | | 1.0 | | 4.3 | 1.1 |
| Cr | | 1.1 | 12.0 | 4.3 | 12.9 | 13.3 |
| Fe | 44.3 | 45.8 | 32.3 | 39.1 | 23.7 | 85.6 |

Figure 11. SEM/LABE image and quantitative EDS data for an area on outside surface of tank cross-section at forward edge of cylindrical section.

4.3.4 SEM/EDS Analyses for Determination of Peak Reentry Temperatures

Samples A1, A3, B, C, and D were selected for SEM/EDS analyses to determine peak reentry temperatures at different locations on the tank surface. These samples were selected because they all appeared to have molten aluminum splatters on the outside surface of the tank. The extent of alloying between the aluminum and stainless steel tank was the basis for the peak temperature estimates. All four samples appeared to have moderate splattering, with the aluminum having a white fluffy appearance, as shown in Figure 12 for Sample B. The tank surface surrounding the aluminum splatters has a rusty appearance due to atmospheric corrosion that occurred after reentry during outdoor storage.



Figure 12. Photograph of Sample B before cutting from region with resolidified metal splatters.

Polished cross-sections of the four samples were examined by optical microscopy to identify areas with possible alloying between the aluminum splatters and stainless steel tank surface. An example of an area selected for analysis is shown in the optical micrograph in Figure 13. This area appeared to have resolidified aluminum splatters on the tank surface and a resolidified area that appeared to be bonded to the tank surface—an indication of alloying between the aluminum and stainless steel. Figure 14 presents a SEM image of the same area, along with EDS elemental maps showing the locations of Al, Fe, and Cr (red, yellow, and green, respectively). The Al map verified the presence of Al splatters on the tank surface. The Fe and Cr maps clearly highlight the stainless steel tank wall. Most importantly, the maps verified the presence of Al, Fe, and Cr within the resolidified material that appeared to have a continuous bond with the tank wall. Thus, the mapping verified alloying between the Al splatters and stainless steel wall, making this a suitable area for more detailed SEM/EDS analyses to determine the peak reentry temperature at this location on the propellant tank.

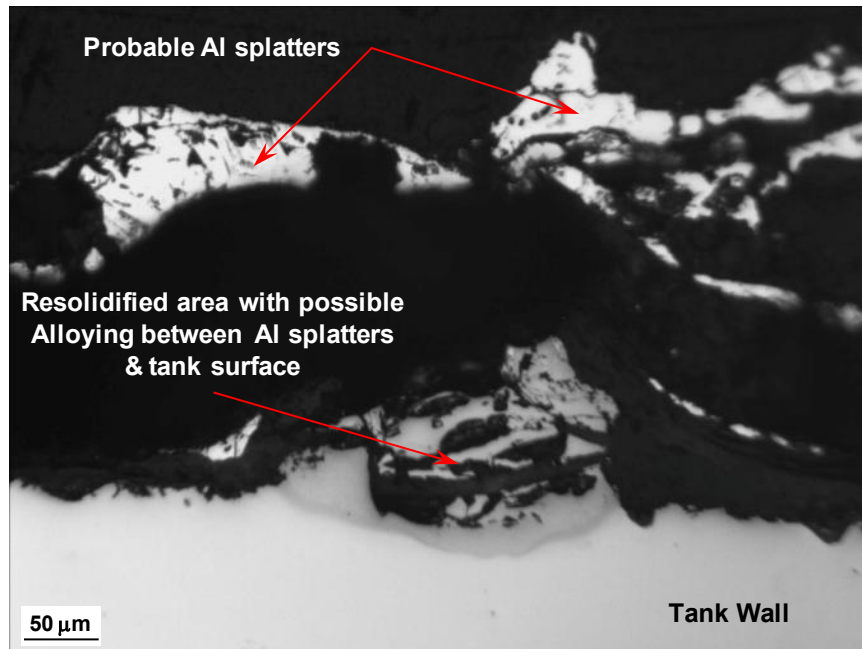


Figure 13. Optical micrograph of cross-section of Sample B showing possible alloying between Al splatters and tank wall.

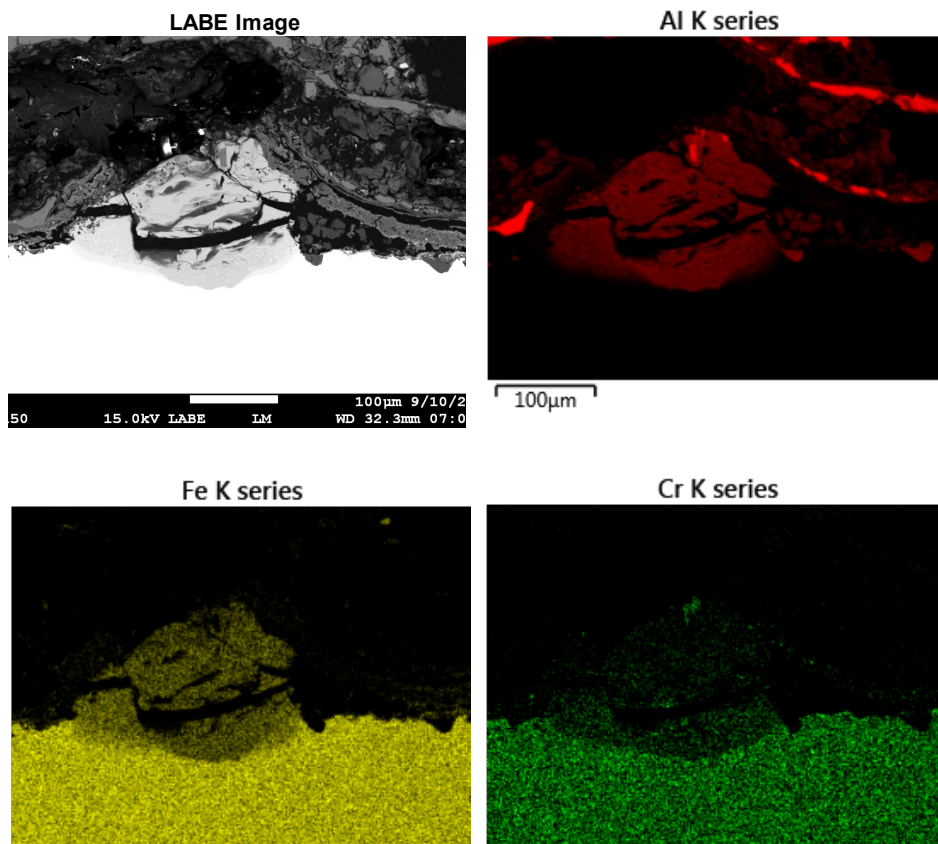


Figure 14. Electron image and elemental maps of area in Figure 13.

A higher magnification SEM/LABE image of the area of interest in Figure 15 shows that the resolidified material consists of a single-phase region and a two-phase region. Both these areas were fully or partially melted at the peak reentry temperature for this location. A region of solid-state diffusion joins the resolidified material to tank wall. The diffusion zone is highlighted by increasing LABE image brightness across the zone from the two-phase region (low atomic mass) to the tank wall (higher atomic mass). The diffusion zone and remaining tank wall did not undergo any melting during reentry.

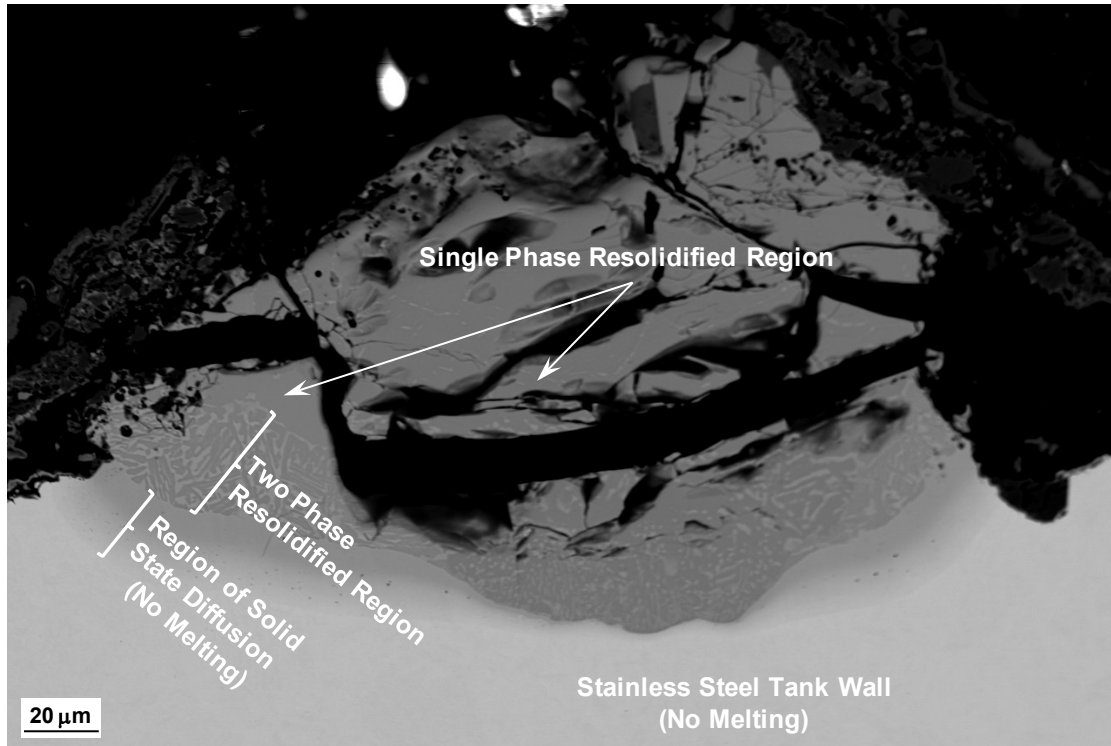


Figure 15. SEM/LABE image of polished cross-section showing region with alloying between Al splatters and tank wall.

Following the procedure used by Wan [3], peak reentry heating was estimated by measuring the compositions of the phases that did and did not melt during reentry and determining their melting temperatures from the Fe–Al phase diagram. The Fe–Al phase diagram was recently updated by Matysik, et al. [10] and is shown in Figure 16. It will be shown below that the area of interest for our analysis is between 50 and 75 at. % Al. This region on the phase diagram is quite complicated near the melting point and is magnified in Figure 17. Depending on the Al concentration, several different intermediate phases (α_2 , ϵ , ξ , η , and ν) can form during cooling between 1200° and 1150°C. All these phases remain stable at room temperature, except for the ϵ phase that decomposes into the α_2 and ξ by the eutectoid reaction at 1092°C.

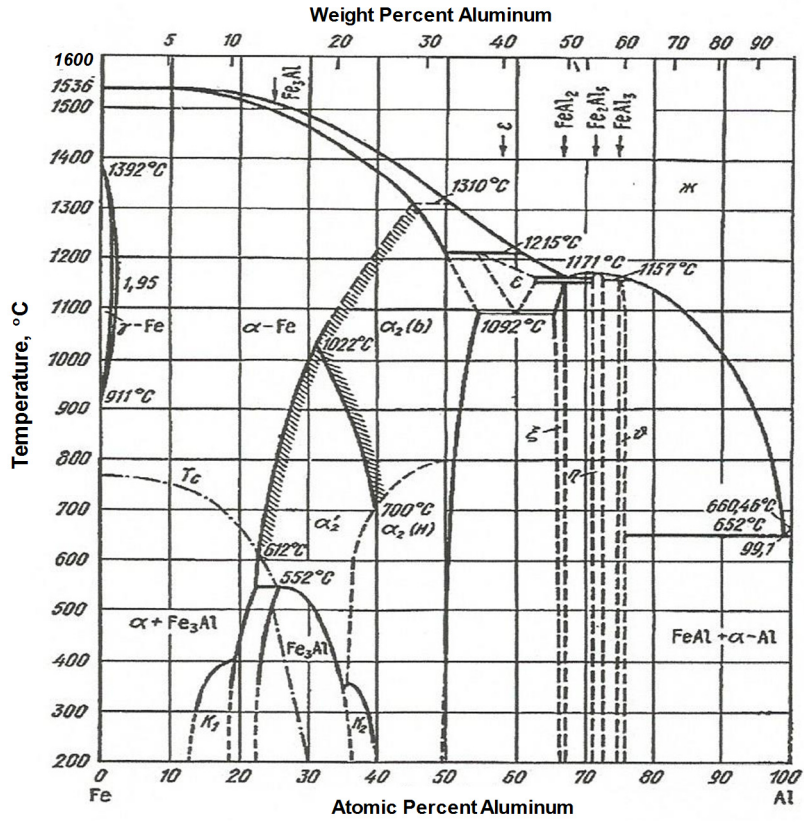


Figure 16. Iron–aluminum phase diagram.

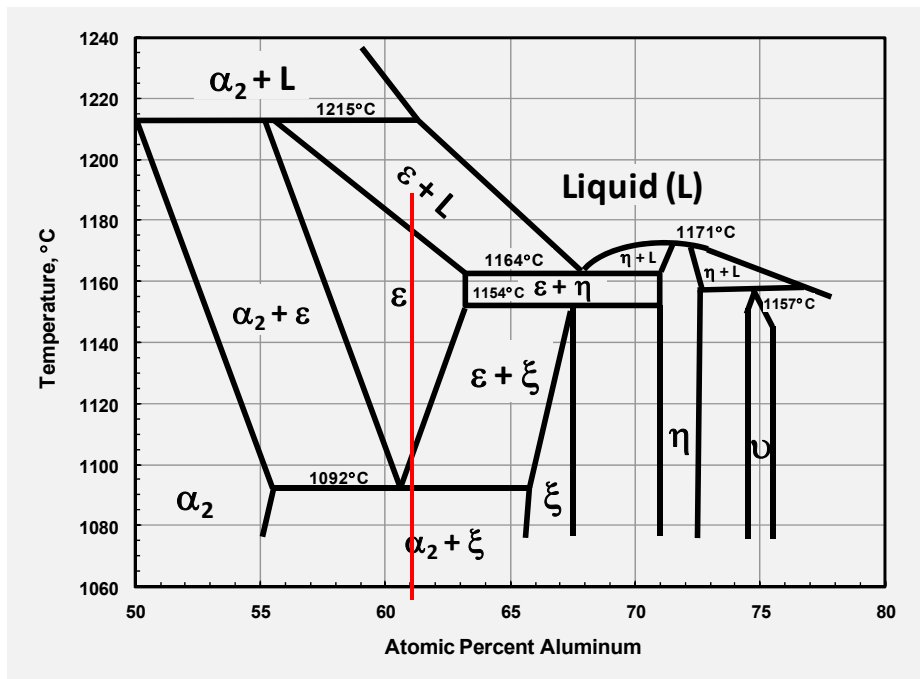


Figure 17. Magnified view of iron–aluminum phase diagram between 50 and 80 at. % Al.

An EDS elemental line scan was made across the diffusion zone, the two-phase resolidified region, and into the single-phase resolidified regions (Figure 15), as shown in Figure 18. The line scan included the elements Al, Si, Cr, Fe, and Mn, but the only elements of interest for our analysis are Al and Fe + Cr. The line scan was initiated within the unalloyed region of the 410 stainless steel, with the typical Fe and Cr compositions of 87 and 13 at. %, respectively. At 13 μm along the scan, the beginning of the diffusion zone was reached, as indicated by slight darkening of LBE image. The Fe and Cr content continually decreased across the diffusion zone while the aluminum content increased. At the end of the diffusion zone just before reaching the two phase resolidified region, the Al content was 53 at. %. This is the maximum Al content for the portion of the tank thickness that did not melt. From the phase diagram (Figure 17), an alloy with 53 at. % Al melts at the peritectic temperature of 1215°C. Thus, the peak reentry temperature at this location on the tank did not exceed 1215°C.

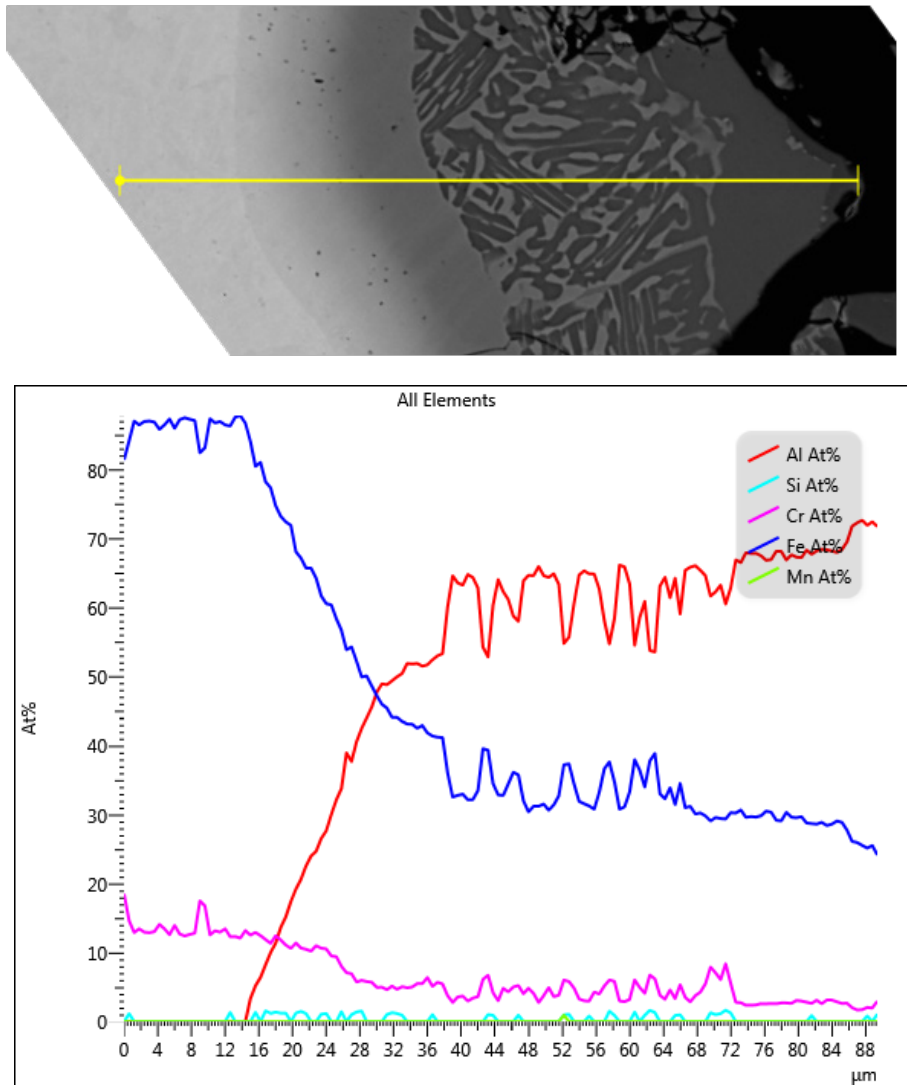


Figure 18. SEM/EDS elemental line across region with alloying between stainless steel tank and aluminum splatters.

As the line scan proceeded across the two-phase region, the Al content varied between approximately 67 and 54 at. %, the respective compositions of the dark and light phases. At approximately 72 μm , the scan entered the single-phase resolidified region, and the Al content stabilized at approximately 67 at. %. A

large area EDS scan of the two-phase resolidified region gave an Al content of 61 at. %, the weighted average for the two phases. From the phase diagram, at temperatures below 1092°C, an alloy with 61 at. % Al (as indicated by the red line) has a microstructure consisting of α_2 with an Al content of approximately 55 at. % (light phase in Figure 18) and ξ with an Al content around 66 at. % (dark phase). For 61 at. % Al, melting initiates at 1075°C. Thus, the peak reentry temperature at this location on the tank was at least 1075°C, but did not exceed 1215°C.

Similar analyses were performed for one area on Sample A3 and five areas on Sample C, as shown in Table 6. Most of these areas had slightly higher aluminum concentrations than the area on Sample B, but the melting temperatures of the resolidified material were similar (1164–1170°C). They all had the same maximum reentry temperature, 1215°C, except for Area 3 on Sample C. There was no apparent diffusion zone at this location, so the only upper limit we could establish was 1520°C, the melting point of 410 stainless steel.

Table 6. Summary of Peak Reentry Temperature Analyses at Several Locations on Mongolia Propellant Tank

| Sample | Area Analyzed | Concentration, at. % Al | | Melting Temperature, °C | |
|--------|---------------|-------------------------|--|-------------------------|--|
| | | Resolidified Area | 1 μm Into Adjacent Area Without Melting | Resolidified Area | 1 μm Into Adjacent Area Without Melting |
| A3 | Area 1 | 71 | 52 | 1170 | 1215 |
| B | Area 2 | 61 | 53 | 1175 | 1215 |
| C | Area 1 Left | 70 | 60 | 1164 | 1215 |
| | Area 1 Right | 68 | 55 | 1164 | 1215 |
| | Area 2 | 70 | 55 | 1164 | 1215 |
| | Area 3 | 70 | 0 | 1164 | 1520 |
| | Area 4 | 70 | 55 | 1164 | 1215 |

Sample B and C came from the forward and aft ends of the cylindrical section, respectively, on the 90° side of the tank. Sample A3 was from the forward dome on the 270° side of the tank. Similar peak temperatures at these locations suggest that the Mongolia tank had uniform reentry heating around the tank, except for locations such as the cylinder edges or melt-through area with special heating conditions. It is concluded that the tank was spinning and/or rotating during reentry, with no apparent preferential orientation. Similar conclusions were reached for the Texas tank [3], which had an estimated reentry temperature of 1200 to 1280°C. It should be noted that Wan used a different version of the iron–aluminum phase diagram for his analysis. When his analysis is repeated using the updated phase diagram (Figures 16 and 17), the reentry temperature range drops to 1164°C to 1250°C.

4.3.5 Additional SEM/EDS Observations

Sample A1, shown in Figure 19, was cut from the aft dome of the propellant tank along the path where the dome fractured during breakup. It was originally cut from the tank for evaluation because the light gray pattern on the outside surface suggested that a thick layer of molten aluminum had splattered along the fracture path during reentry. However, once the sample was removed, it was discovered that a matching gray pattern was also present on the inside surface (Figure 20). SEM/EDS spectra were taken on the surfaces of the gray area as well as the reddish area. No aluminum was detected on the gray area, and

both surface areas were predominantly iron and oxygen. The reddish iron oxide was representative of most of the tank surface, resulting from atmospheric corrosion due to outdoor storage following reentry.



Figure 19. Photograph of Sample A1 secured to aft dome by binder clips after removal from Mongolia tank.

X-ray diffraction spectra were taken for the gray and reddish areas to further characterize the oxide layers. Magnetite (Fe_3O_4) or maghemite ($\gamma\text{-Fe}_2\text{O}_3$) and lepidocrocite ($\text{FeO}(\text{OH})$) matched the spectra for the reddish area (Figure 21). Magnetite and maghemite have the same diffraction peaks, so either or both oxides may have been present. However, maghemite is normally not stable at room temperature, so the reddish oxide is likely magnetite [11].

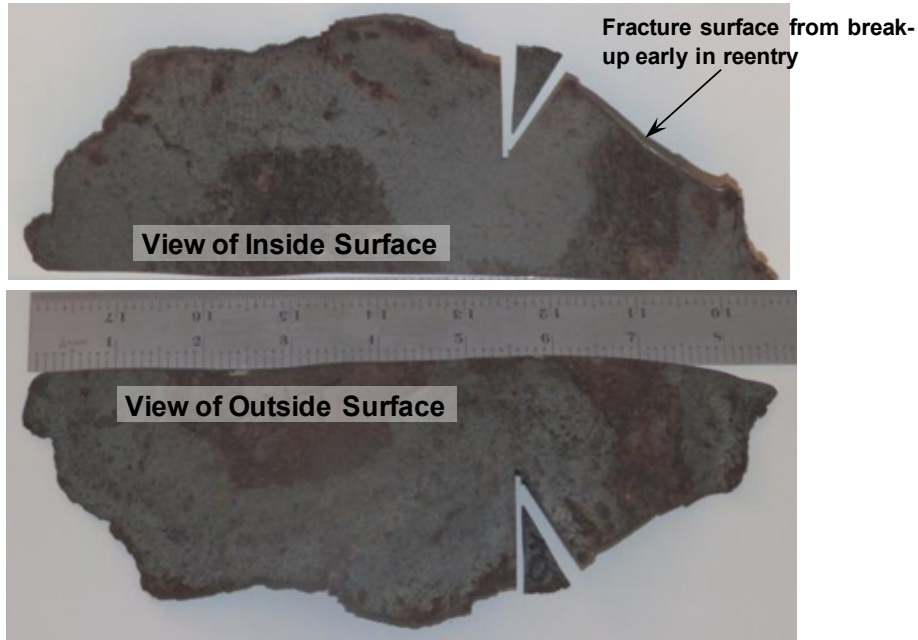


Figure 20. Photographs of outside and inside surfaces of Sample A1.

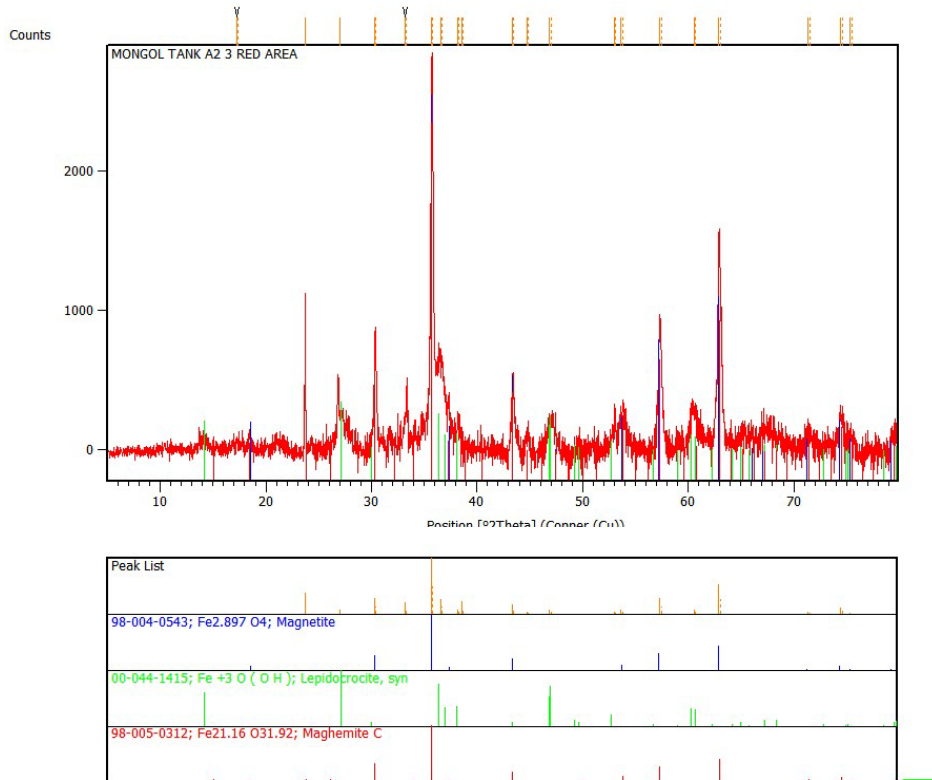


Figure 21. X-ray diffraction spectrum obtained from reddish oxide on Sample A1.

Figure 22 shows the diffraction pattern for the gray area. Magnetite and/or maghemite plus hematite (α -Fe₂O₃) matched the diffraction peaks. Hematite and magnetite are both stable at room temperature, and the gray area is likely a combination of these two oxides. At temperatures below 570°C, iron oxidizes

with an inner layer of magnetite and outer layer of hematite [11]. Therefore, hematite probably caused the gray color. Similar color patterns were observed at a few locations along the forward and aft edges of the cylindrical section. Thus, it was only observed near tank edges. It was assumed that the hematite formed during reentry, but only at locations having favorable temperature and air flow characteristics.

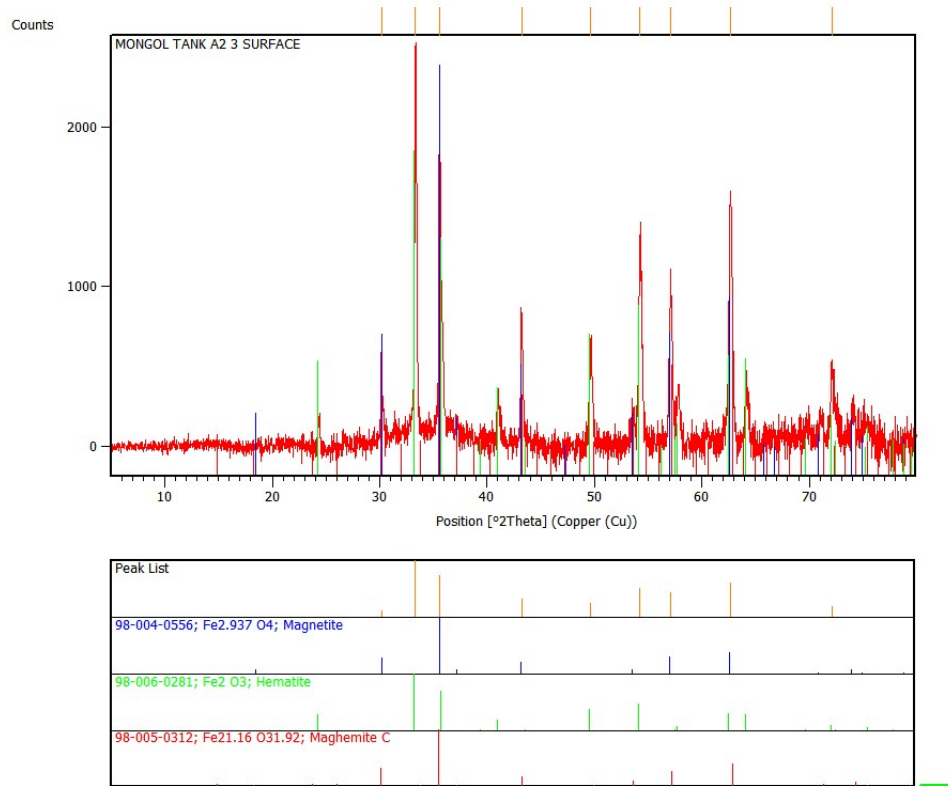


Figure 22. X-ray diffraction spectrum obtained from gray oxide on Sample A1.

Molten metal splatters on the Mongolia tank were primarily aluminum, with small concentrations of common aluminum alloying elements such as magnesium and silicon. Copper was also detected by SEM/EDS at several locations. Figure 23 is a LAME image of a typical area with Cu-rich particles on the cross section of Sample A3. The particle on the left was 70 at. % Cu and 25 % Al and the other two particles were 45 at. % Cu + 40 % Al + 10 % Fe. All the splatters observed with high copper concentrations also had significant aluminum concentrations. However, we were primarily looking at cross-sections of areas with obvious aluminum splatters. Thus, it is quite possible that copper splatters were present at other locations in the absence of any aluminum. For the samples that were analyzed, Cu-rich particles were usually on the surface of the resolidified aluminum splatters, but were occasionally imbedded in the Al-rich layer. The Cu-rich particles were usually similar in size (10–20 μm across) to those in Figure 23, but often had a more irregular cross-section than did the round particles in the figure. The copper probably originated from electrical wiring attached to propellant tank that melted and splattered onto the tank surface.

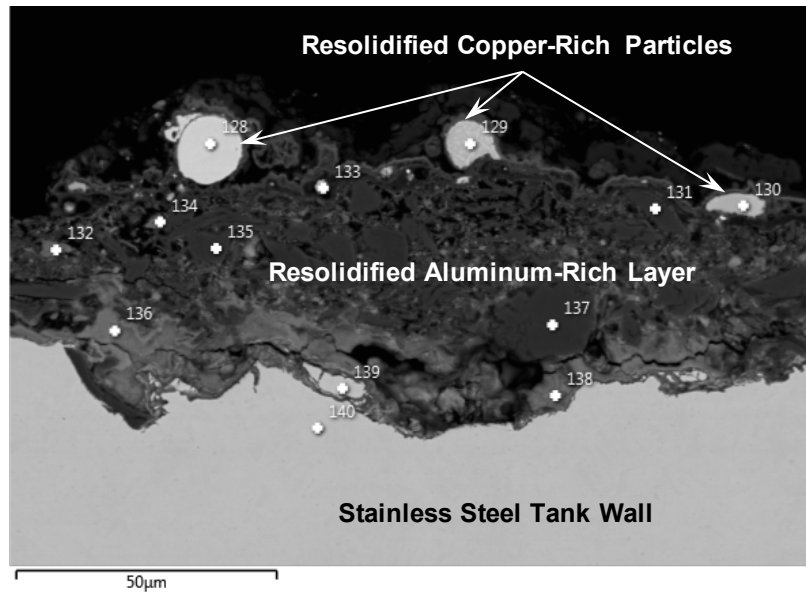


Figure 23. LBE image of Cu-rich particles on top of aluminum splatters on Sample A3.

5. Summary and Conclusions

The objectives of this investigation were to document visible reentry damage to the Delta II Stage 2 propellant tanks that landed in South Africa and Mongolia, to perform laboratory analyses on the Mongolia tank to characterize reentry damage and determine peak reentry temperatures, and to compare reentry damage to the propellant tanks that landed in Texas, South Africa, and Mongolia. These objectives were achieved, as highlighted below.

The Texas and South Africa propellant tanks were flat on one side from Earth impact, but maintained the basic cylindrical shape, with domed ends over the rest of their surface areas. Both tanks had clean separations during reentry breakup from the thrust chamber and Aerojet AJ10-118K engine at the bolted connection to the aft flange. For the Mongolia tank, it appeared that most of the aft dome was ripped away from the propellant tank, along with the thrust chamber and engine during breakup. Consequently, the Mongolia tank had diminished structural integrity and suffered more significant deformation upon Earth impact than did the Texas and South Africa tanks. The aft dome and cylindrical section on the impact side of the tank collapsed into a concave geometry, with the interior bulkhead pushed out through the opening at the aft end.

Common observations for the Texas, South Africa, and Mongolia included complete removal of the pale-green primer coating from the exterior surface, molten metal splatters at numerous locations on the tank surfaces, and localized melting along portions of the forward and aft ends of the cylindrical section due to enhanced aerodynamic heating at the exposed edges.

Multiple micrometeoroid impact craters were observed on the Texas and South Africa propellant tanks. No impact craters were found on the Mongolia tank.

A large melt-through hole, approximately 0.5 m^2 , was observed on the forward dome for the Texas and Mongolia propellant tanks. SEM/EDS analyses of resolidified metal around the perimeter of the hole for the Mongolia tank were consistent with those reported by Wan [3] for the Texas tank. From the presence of large quantities of oxidized aluminum on the outer surface, Wan theorized that the localized melting was caused by the build-up of molten aluminum on the tank surface, which rapidly oxidized in the air stream and caught on fire, thereby producing enough heat to melt the stainless steel tank wall. It was concluded that this same mechanism applied for the Mongolia tank.

The detailed photographs of the South Africa propellant tank showed no evidence of any melt-through holes. In addition to the Texas and Mongolia propellant tanks, post-reentry melt-through holes attributed to the burning aluminum mechanism have been observed on five Delta II Upper Stage titanium alloy motor cases [7][8]. Thus, the South Africa tank is the first of eight Delta II propellant tanks or motor cases analyzed after reentry that did not have any large melt-through holes.

Peak reentry temperatures were estimated at two locations on the same side (but opposite ends) of the cylindrical section and one location on the forward dome of the Mongolia propellant tank. The area of the forward dome was 180° around the tank from the areas on the cylindrical section. Similar reentry temperatures of at least 1164°C —but less than 1215°C —were estimated for the three locations. It was concluded that the tank had uniform reentry heating around its exterior, except for locations such as the cylinder edges or melt-through areas with special heating conditions. It is concluded that the tank was spinning and/or rotating during reentry with no apparent preferential orientation. Similar conclusions were reached for the Texas tank [3], which had similar estimated peak reentry temperatures.

The Texas and Mongolia propellant tanks had a dark rust and rough appearance versus a lighter brown color and smoother surface for the South Africa tank. The 410 stainless steel alloy has a martensitic structure that is susceptible to atmospheric corrosion. The Texas and Mongolia tanks were stored outdoors before and after delivery to Aerospace, while the South Africa tank was relocated indoors at SAAO shortly after recovery. Thus, the rusty appearance of the Texas and Mongolia tanks was indicative of their post-reentry storage history.

This investigation successfully characterized reentry damage and provided qualitative peak reentry temperatures that can be utilized by analysts to validate, refine, and calibrate reentry models used for reentry risk assessments.

6. References

- [1] Graham, W., “ULA Successfully Launches STSS-Demo via Delta II,” *NASA Spaceflight.com*, 25 September 2009.
- [2] Reichel, D. H., “Pick-up of Mongolian Debris,” email message to T. T. Huynh, USAF AFSPC SMC/LRE, 17 May 2011.
- [3] Wan, C. C., Metallurgical Investigation of a Reentered Delta II Stage II Propellant Tank, ATR-2003(9368)-3, The Aerospace Corporation, 31 August 2003.
- [4] Botha, W., “Orbital Debris: A Case Study of an Impact Event in South Africa,” *Proceedings of the Third European Conference on Space Debris, 19 – 21 March 2001, Darmstadt, Germany*, ESA SP-473, Vol 2, Edited by H. Sawaya-Lacoste, Noordwijk, Netherlands: ESA Publications Division, ISBN 92-9092-733-X, pp. 501 – 506.
- [5] Metals Handbook Vol. 8, “Metallography, Structures, and Phase Diagrams,” 8th Edition, American Society for Metals, Metals Park, OH, 1973.
- [6] Wan, C. C., Uht, J. C. and Patel, D. N., *Metallurgical Investigation of a Reentered Delta II Upper Stage Star 48 Propellant Tank*, ATR-2004(9368)-4, The Aerospace Corporation, 25 June 2004.
- [7] Steckel, G. L., Metallurgical Evaluation of Reentry Effects on Delta II Upper Stage Star 48 Motor Cases, TOR-2009(8506)-13, The Aerospace Corporation, 30 December 2009.
- [8] Steckel, G. L., Summary of Reentry Effects on Five Delta II Upper-Stage Star 48 Motor Cases, TOR-2016-02193, The Aerospace Corporation, 30 June 2016.
- [9] *Martensitic Stainless Steels Types 410, 420, 425 Mod, and 440A*, Allegheny Ludlum Technical Data Blue Sheet B175/ED1/998/SW, Allegheny Ludlum Corporation, Pittsburgh, PA, 1998.
- [10] P. Matysik, S. Jozwiak, and T. Czujko, “Characterization of Low-Symmetry Structures from Phase Equilibrium of Fe-Al System—Microstructures and Mechanical Properties,” *Materials*, vol. 8, 2015, pp. 914–931.
- [11] N. Bertrand, C. Desgranges, D. Poquillon, M. C. Lafont, and D. Monceau, “Iron Oxidation at Low Temperature (260–500°C) in Air and the Effect of Water Vapor,” *Oxidation of Metals*, vol. 73 (n° 1–2) pp. 139–162.

Technical Reports Addendum Asset Summary #2018013110245414334

Report Name: Evaluation of Reentry Effects on Delta II Second Stage Propellant Tanks

Aerospace Report Number: TOR-2018-00670

JO: 8506-22

First Aerospace Author / PI: Steckel, Gary L

Created By: Gary L Steckel

NON Aerospace MTE: *No assets reported.*

ABB367 PANALYTICAL X/Pert Pro MPD

Usage Dates: 08/01/2015 - 03/31/2017

| Calibration Date | Calibration Due Date | Certificate Number | Certificate Notes |
|------------------|----------------------|----------------------------------|-------------------|
| 07/20/2015 | Not Applicable | ABB367:1437376359 | SAE* |
| 08/03/2015 | 02/26/2017 | 5cb01dfc2865ba44bc792b1fe762a05c | TMT-NORMAL |
| 02/27/2017 | 01/27/2019 | b528544217484d40a6598b3b6080ca84 | TMT-NORMAL |

*Support and Auxillary Equipment are not calibrated.

ACR364 JEOL (USA) INC. JSM-7600F

Usage Dates: 08/01/2015 - 03/31/2017

| Calibration Date | Calibration Due Date | Certificate Number | Certificate Notes |
|------------------|----------------------|----------------------------------|-------------------|
| 07/08/2015 | 03/05/2017 | 7ad3f47855c56647972e2f82b9147377 | TMT-NORMAL |
| 03/14/2017 | 03/10/2019 | 7786d2c811e86c4a9185acbbb71ed80c | TMT-NORMAL |

Technical Reports Addendum Asset Summary #2018013110245414334

ACR429 OXFORD INSTRUMENTS X-MAX

Usage Dates: 08/01/2015 - 03/31/2017

| Calibration Date | Calibration Due Date | Certificate Number | Certificate Notes |
|------------------|----------------------|----------------------------------|-------------------|
| 06/02/2014 | 12/27/2015 | f840182f4f92e2449d541c92c3465ec2 | TMT-NORMAL |
| 12/22/2015 | 11/19/2017 | af364ce3cb2a1d4c857c7a74a8dc2952 | TMT-NORMAL |

ACT192 MITUTOYO CD-8CX

Usage Dates: 08/01/2015 - 03/31/2017

| Calibration Date | Calibration Due Date | Certificate Number | Certificate Notes |
|------------------|----------------------|----------------------------------|-------------------|
| 01/20/2015 | 08/14/2016 | ba1f12da7bf0a84684ecb00d1ab893b5 | TMT-NORMAL |
| 09/15/2016 | 08/12/2018 | 41ab50a5f2121b4c987a59b8e276743f | TMT-NORMAL |

ACT193 MITUTOYO 293-344

Usage Dates: 08/01/2015 - 03/31/2017

| Calibration Date | Calibration Due Date | Certificate Number | Certificate Notes |
|------------------|----------------------|----------------------------------|-------------------|
| 01/12/2015 | 08/07/2016 | 8301c1795af32a4894ecf0b506cc5da5 | TMT-NORMAL |
| 09/15/2016 | 08/12/2018 | a34aaddf497ab04b928dc57107b9ba36 | TMT-NORMAL |

AH488 ROCKWELL 3JS

Usage Dates: 08/01/2015 - 03/31/2017

| Calibration Date | Calibration Due Date | Certificate Number | Certificate Notes |
|------------------|----------------------|----------------------------------|-------------------|
| 09/30/2014 | 09/25/2016 | ef9ee70d031fd644b7b68b8b3bc86eb1 | TMT-NORMAL |
| 10/20/2015 | 10/15/2017 | 38e1631f89e48d46bbe2261afbbb797a | TMT-NORMAL |

Technical Reports Addendum Asset Summary #2018013110245414334

CL269 NIKON INC. EPIPHOT

Usage Dates: 08/01/2015 - 03/31/2017

| Calibration Date | Calibration Due Date | Certificate Number | Certificate Notes |
|------------------|----------------------|----------------------------------|-------------------|
| 05/29/2013 | Not Applicable | 709ab69242deb34e8fa622102b567f6b | SAE* |

*Support and Auxillary Equipment are not calibrated.

External Distribution

REPORT TITLE

Evaluation of Reentry Effects on Delta II Second Stage Propellant Tanks

REPORT NO.

TOR-2018-00670

PUBLICATION DATE

February 12, 2018

SECURITY CLASSIFICATION

UNCLASSIFIED

Jesse Edwards
AFSMC
Jesse.Edwards@losangeles.af
.mil

Dan H. Reichel
ManTech
Dan.Reichel@ManTech.com

M. Glissman
HQ Air Force Safety Center
(AFSC/SES)
mark.glissman.1@us.af.mil

P. D. Wilde
Federal Aviation
Administration
paul.wilde@faa.gov

Thomas Huynh
AFSMC
Thomas.Huynh@losangeles.a
f.mil

J. C. Liou
NASA Johnson Space Center
jer-chyi.liou-1@nasa.gov

Tobias Lips
HTG - Hyperschall
Technologie Gottingen
T.Lips@htg-hst.de

APPROVED BY _____
(AF OFFICE)

DATE _____

Evaluation of Reentry Effects on Delta II Second Stage Propellant Tanks

Approved Electronically by:

Rafael J. Zaldivar, DIRECTOR DEPT
MATERIALS SCIENCE DEPT
SPACE MATERIALS LABORATORY
ENGINEERING & TECHNOLOGY GROUP

Cognizant Program Manager Approval:

Vale T. Sather, SYSTEMS DIRECTOR
SYSTEMS & SOFTWARE ENGINEERING
ENGINEERING AND MISSION READINESS
SPACE SYSTEMS GROUP

Aerospace Corporate Officer Approval:

Malina M. Hills, SR VP SPACE SYS
SPACE SYSTEMS GROUP

Content Concurrence Provided Electronically by:

Gary L. Steckel, MTS RET CASUAL R3
METALS/CERAMICS
MATERIALS SCIENCE DEPT
ENGINEERING & TECHNOLOGY GROUP

© The Aerospace Corporation, 2018.

All trademarks, service marks, and trade names are the property of their respective owners.

PK2099